JCI The Journal of Clinical Investigation

Pro-inflammatory P2Y14 receptor inhibition protects against ischemic acute kidney injury in mice

Maria Agustina Battistone, … , Dennis Brown, Sylvie Breton

J Clin Invest. 2020. https://doi.org/10.1172/JCI134791.

Research In-Press Preview Inflammation Nephrology

Graphical abstract

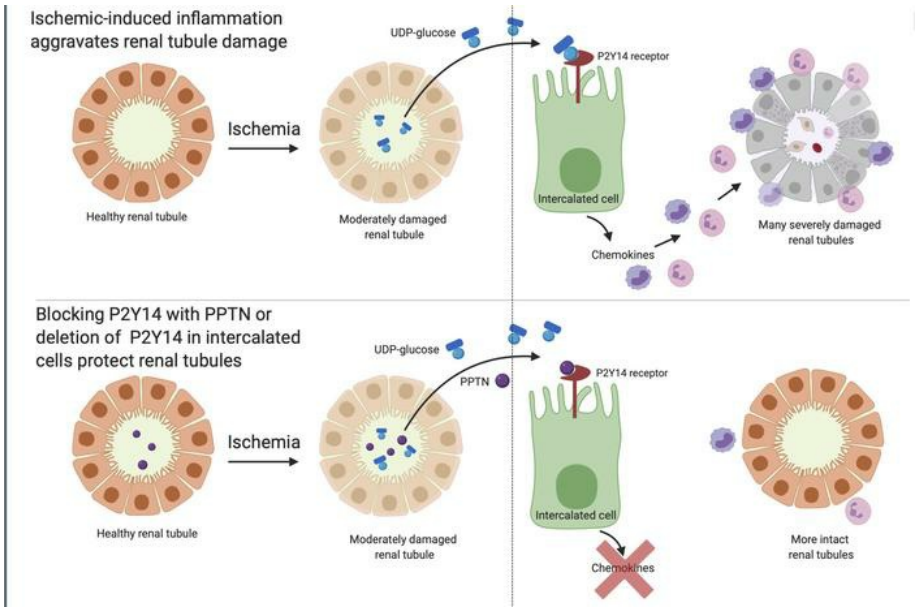

Pro-inflammatory P2Y14 receptor inhibition protects against ischemic acute kidney injury in mice

Maria Agustina Battistone[1], Alexandra C. Mendelsohn[1], Raul German Spallanzani[2], Andrew S. Allegretti[3], Rachel N. Liberman[1], Juliana Sesma[4, 5], Sahir Kalim[3], Susan M. Wall[6], Joseph V. Bonventre[7], Eduardo R. Lazarowski[4], Dennis Brown[1] and Sylvie Breton[1]

[1] Program in Membrane Biology, Division of Nephrology, Department of Medicine, Massachusetts General Hospital and Harvard Medical School, Boston, MA, MA 02114, USA
[2] Division of Immunology, Department of Microbiology and Immunobiology, Harvard Medical School, and Evergrande Center for Immunologic Diseases, Harvard Medical School and Brigham and Women's Hospital, Boston, MA, USA.
[3] Division of Nephrology, Department of Medicine, Massachusetts General Hospital, Boston, MA 02114, USA
[4] Department of Medicine, Marsico Lung Institute. University of North Carolina. Chapel Hill, NC, USA
[5] Current address: CONICET, Facultad de Ciencias Médicas, Universidad Nacional de Rosario, Rosario, Argentina.
[6] Renal Division, Department of Medicine, Emory University School of Medicine, Atlanta, GA, USA
[7] Division of Renal Medicine and Division of Engineering in Medicine, Brigham and Women's Hospital and Harvard medical School, MA 02115

Correspondence: Sylvie Breton, PhD
Simches Research Center
185 Cambridge St. Suite 8.204
Boston, MA 02114
Email: Breton.sylvie@mgh.harvard.edu

ABSTRACT

Ischemic acute kidney injury (AKI), a complication that frequently occurs in hospital settings, is often associated with hemodynamic compromise, sepsis, cardiac surgery or exposure to nephrotoxicants. Here, using a murine renal ischemia-reperfusion injury (IRI) model we show that intercalated cells (ICs) rapidly adopted a pro-inflammatory phenotype post-IRI. During the early phase of AKI, we demonstrate that either blocking the pro-inflammatory P2Y14 receptor located on the apical membrane of ICs, or ablation of the gene encoding the P2Y14 receptor in ICs: 1) inhibited IRI-induced chemokine expression increase in ICs; 2) reduced neutrophil and monocyte renal infiltration; 3) reduced the extent of kidney dysfunction; and 4) attenuated proximal tubule (PT) damage. These observations indicate that the P2Y14 receptor participates in the very first inflammatory steps associated with ischemic AKI. In addition, we show that the concentration of the P2Y14 receptor ligand, uridine diphosphate-glucose (UDP-Glc), was higher in urine samples from intensive care unit patients who developed AKI compared to patients without AKI. In particular, we observed a strong correlation between UDP-Glc concentration and the development of AKI in cardiac surgery patients. Our study identifies the UDP-Glc/P2Y14 receptor axis as a potential target for the prevention and/or attenuation of ischemic-AKI.

INTRODUCTION

Acute kidney injury (AKI) is a frequent medical complication seen in hospitalized patients. It is associated with an increased length of hospital stay, the development of chronic kidney disease (CKD), and increased risk of mortality (1-4). Over the past decades the rates of AKI have progressively increased worldwide, making AKI a growing health care burden (3, 5, 6). Unfortunately, there is no targeted therapy for hospital acquired AKI other than avoiding potential nephrotoxins and hemodynamic optimization (7-9).

AKI is the consequence of either a direct insult to the kidney or a distant organ, and multiple primary medical conditions are associated with AKI (10-16). AKI is often associated with renal ischemia, which occurs in the context of multiple organ failure, sepsis, and vascular occlusion (17). Ischemic AKI is particularly common during cardiac surgery requiring cardiopulmonary bypass (CPB) (12, 18-21). The loss of kidney function is frequently associated with infiltration of circulating innate immune cells into the renal tissue (14, 22-26). This results in an inflammatory cascade that enhances and even causes kidney injury, and is rapidly followed by a progressive decline in renal blood flow and glomerular filtration rate (GFR), and acute tubular injury (4, 27-29). Renal inflammation is associated with both septic- and non-septic AKI (30), and recent evidence has indicated that activation of innate immunity itself is sufficient to cause AKI (14). In particular, the AKI that follows ischemia-reperfusion-injury (IRI) is associated with infiltration of inflammatory cells into the kidney stroma (17, 27, 31). Danger-associated-molecular-pattern (DAMP) molecules are released following tissue stress or injury and activate pattern recognition receptors (PRRs), which initiates sterile inflammation (14, 32-34). Activation of PRRs by DAMPS induces the production of chemokines, which attract neutrophils and monocytes to the site of

inflammation (14). Newly recruited neutrophils and monocytes produce cytotoxic substances such as reactive oxygen species, and they cause microvasculature congestion, which ultimately impairs renal blood flow creating a sustained ischemic insult (14). This first wave of immune cell infiltration occurs rapidly after injury (27). As such, blockade of this very first step in the inflammatory cascade may offer therapeutic benefits (7, 8, 14).

DAMPs include, but are not limited to, high-mobility group protein B1 (HMGB1), ATP, DNA and uridine diphosphate-glucose (UDP-Glc) (34-39). UDP-sugars are components of glycosylation reactions, but they can also act as potent agonists of the pro-inflammatory P2Y14 receptor when secreted from injured cells (35, 40-44). Whereas most nucleotides, such as ATP, are rapidly degraded by ectonucleotidases after their release, extracellular UDP-Glc exhibited high stability in most tissues and cell types investigated (37, 43-45). This high stability of UDP-Glc provides a mechanism by which the release of UDP-sugars from stressed cells could lead to elevated extracellular concentrations (35), leading to pro-inflammatory receptor activation. The UDP-Glc sensing P2Y14 receptor is expressed in several tissues including the lung and uterus, and epithelial cells can be initiators of inflammation in these organs (35, 41, 46). Elevated UDP-Glc levels and increased numbers of neutrophils were observed in sputum samples from cystic fibrosis patients with moderate or severe lung injury compared to control subjects, and intratracheal instillation of UDP-Glc in mice promoted neutrophil migration into the lung, indicating a link between UDP-Glc and inflammation (43). Similarly, injection of UDP-Glc into the mouse uterus induced a 5-fold increase in the number of neutrophils present in the endometrium (41). Furthermore, we previously showed that collecting duct intercalated cells (ICs) are sensors of UDP-Glc and mediate the recruitment of neutrophils into the kidney via activation of the P2Y14 receptor located on their apical membrane (42, 47).

Here, we used renal IRI as a mouse model of AKI (48) to examine the role of the UDP-Glc/P2Y14 receptor signaling pathway in the pathogenesis of the renal inflammation that leads to kidney injury. Our study shows that blocking the P2Y14 receptor with a selective inhibitor, or ablation of the P2Y14 receptor gene in ICs reduced renal inflammation, attenuated proximal tubule (PT) damage and improved kidney function following renal IRI. Finally, in a pilot study, we observed that urine UDP-Glc levels strongly correlated with the incidence of AKI in intensive care unit (ICU) and cardiac surgery patients. This study, therefore, identifies the UDP-Glc/P2Y14 receptor pathway as a potential therapeutic target, which might be used to prevent or alleviate IRI-induced AKI.

RESULTS

Elevated urine UDP-Glc after renal IRI in mice

Transgenic male mice that express EGFP under the control of the promoter of the IC specific V-ATPase B1 subunit (ATP6V1B1) gene (B1-EGFP) were subjected to bilateral renal IRI or sham surgery, and they were put in metabolic cages in groups of 3 mice (except for the 2h post-IRI group). Urine was collected for the first 2h, 24h and 48h post-operatively. UDP-Glc was measured by LC-MS/MS and urinary values were normalized for urine creatinine (uCre). We observed a significant increase in the urinary UDP-Glc/uCre ratio in the mice undergoing IRI relative to SHAM during the first 2h after IRI. After 24h and 48h, the urine UDP-Glc/uCre ratios in the IRI groups were similar to the ratios observed in the SHAM groups (Fig. 1).

Intercalated cells acquire a pro-inflammatory phenotype after IRI

To determine the response of ICs to experimental IRI, we evaluated their expression of selected pro-inflammatory transcripts by qPCR. EGFP-positive ICs were isolated by fluorescence activated cell sorting (FACS) from the kidney medulla of B1-EGFP mice 2h, 4h and 24h after IRI or sham surgery (Fig. 2A). We selected the medulla in order to avoid the isolation of cortical connecting segment cells, which also express EGFP in these mice. We observed up-regulation of several chemokines including *Cxcl1, Cxcl2,* and *Ccl2* as early as 2h after IRI (Fig. 2B). *Cxcl2* remained elevated up to 24h after IRI. The complete gene expression profile of isolated ICs was, therefore, characterized at 2h post-IRI by RNA-sequencing (RNA-seq). The complete transcriptome dataset is shown in Suppl. Table 1. Volcano plots (fold change (FC) versus P value) compare the gene expression profiles of ICs, 2h after IRI *versus* SHAM, and show increased expression of several pro-inflammatory genes, including *P2ry14* itself, as well as *CxCl1*, *Cxcl2, Cxcl3,*

Cxcl5, Cxcl10, Ccl17, Il-1β, Il-6, and *Il-34* (Fig. 2C). The complete list of genes up-regulated after IRI is provided in Suppl. Table 2, where pro-inflammatory transcripts are indicated in red. A list of selected genes that were down-regulated after IRI is provided in Suppl. Table 3. These latter include genes involved in DNA replication, mismatch repair, and metabolism of pyrimidine, glycine, serine and threonine.

Participation of the P2Y14 receptor in the pro-inflammatory response of ICs

To determine whether the pro-inflammatory response of ICs might be related to the increase in urinary UDP-Glc after IRI, we next used a potent and highly selective antagonist of the P2Y14 receptor, PPTN (4,7-disubstituted 2-naphthoic acid derivative) (42, 49, 50) as a means of inhibiting the activation of IC-specific chemokine expression induced by IRI. Because the P2Y14 receptor is located on the apical membrane of ICs (42), and because PPTN and UDP-Glc compete for a common P2Y14 extracellular binding site (35), we first determined whether PPTN is excreted intact into the urine. To do so, urine samples were collected following PPTN administration to mice (Fig. 3A). PPTN was detected intact in the urine by LC-MS/MS, and its concentration was 87.8 ± 24.1 nM 2h after mice received a single I.V. injection corresponding to the dose of 0.18 mg/kg. A constant higher concentration at around 200 nM was detected at 24h and 48h when mice received a daily dose of 4.55mg/kg via osmotic minipumps. Control mice received equivalent amounts of the vehicle, DMSO.

To determine whether PPTN could modulate the IC inflammatory response induced by IRI, chemokine expression was assessed by qPCR in ICs isolated by FACS from B1-EGFP mice treated with PPTN or vehicle. ICs were isolated 2h after IRI or SHAM procedure. Figure 3B shows that PPTN treatment significantly reduced the increase in IC-specific chemokine expression induced

by IRI. No difference in chemokine expression was detected between the SHAM-DMSO and SHAM-PPTN groups, and these two groups were, therefore, combined into a single SHAM group in the graph.

Prophylactic inhibition of the P2Y14 receptor reduces renal pro-inflammatory immune cell recruitment after IRI

Renal infiltration of immune cells was quantified by flow cytometry analysis in mice subjected to bilateral IRI. IRI induced significant recruitment of $CD45^+$ immune cells (Fig. 4A), including $CD45^+CD11b^+Ly6G^+$ cells with a "neutrophil" phenotype (Fig. 4B), and $CD45^+CD11b^+Ly6C^+$ cells with a "monocyte" phenotype (Fig. 4C) into the kidney tissue as early as 2h after surgery. In contrast, PPTN treatment significantly reduced the recruitment of immune cells, neutrophils and monocytes even at this early time point (Fig. 4A-C). Neutrophil and monocyte recruitment was also lower in the PPTN-treated group compared to the vehicle-treated group 24h after IRI (Fig. 4D, 4E). However, by 48h after IRI, neutrophil and monocyte numbers had returned to baseline with values similar in PPTN- and vehicle-treated mice (Fig. 4E).

Prophylactic inhibition of the P2Y14 receptor reduces the extent of kidney dysfunction after IRI

Further studies explored whether PPTN treatment attenuated the fall in renal function and the rise in markers of kidney injury that follow AKI. Serum creatinine (sCr), blood urea nitrogen (BUN), albuminuria, and the PT injury urine marker KIM-1 were assessed in control mice (SHAM) and mice subjected to renal bilateral IRI. A significant elevation of sCr and BUN was observed following IRI in vehicle-treated mice, as previously shown by several laboratories (51, 52) (Fig. 5A, B). Mice treated with PPTN showed a significant reduction in sCr and BUN compared to the

SHAM group, indicating preservation of kidney function after IRI. No effect of PPTN was observed at the early 2h time point, indicating intrinsic damage caused by ischemia, and sCre did not go up above this initial elevation 24h and 48h post-IRI. IRI also caused albuminuria (Fig. 5C) and elevation of KIM-1 urinary concentration (Fig. 5D) indicating damage to PTs (53, 54), which are known to be among the most affected tubules after IRI. However, PPTN treatment significantly attenuated albuminuria severity and KIM-1 elevation 48 h after IRI, showing preservation of PT function (Fig. 5C and D).

Prophylactic inhibition of the P2Y14 receptor reduces kidney damage after IRI

Histopathological examination of kidney sections stained using hematoxilin & eosin (H&E) was conducted to determine the effect of PPTN on kidney tubules following IRI versus SHAM. As shown in Fig. 6A, many damaged PTs were detected 24h and 48h after IRI compared to SHAM in vehicle-treated mice (left panels). A reduction in the number of damaged PTs was observed in the PPTN-treated groups (right panels) compared to vehicle-treated groups. This protection was observed 24h and 48h after IRI. No effect of PPTN was observed in the SHAM group (compare top right and top left panels). We quantified the number of intact, moderately damaged and very damaged renal tubules, as shown in Fig. 6B. The percentage of intact tubules significantly increased in the PPTN group compared to DMSO at 48h post-IRI. This was accompanied by a significant reduction in the number of very damaged tubules at 24h.

Protection by PPTN following IRI was also demonstrated in kidney sections labeled using phalloidin-Alexa 647, a marker of F-actin. IRI induced a marked actin depolymerization in the brush-border membrane and along the basolateral membrane of PT cells 24h and 48h after IRI (Suppl. Fig. 1A, left panels), as previously shown in rats (55). In the treated group, intact brush-

border membrane and basolateral staining was detected indicating preservation of the actin cytoskeleton in PT cells (Suppl. Fig. 1A, right panels). Similarly, labeling for the PT specific scavenger receptor, megalin, showed loss of apical membrane after IRI (Suppl. Fig. 1B, left panels), and marked protection by PPTN 24h and 48h after IRI (Suppl. Fig. 1B, right panels). To further assess PT cell polarity, we labeled kidney sections for aquaporin 1 (AQP1), which is located in the brush-border and basolateral membrane of intact PT cells (56). IRI induced the redistribution of AQP1 from the plasma membrane into the entire cell body in PTs 24h and 48h after IRI (Fig. 7A, left panels). This intracellular AQP1 redistribution was less pronounced in the PPTN-treated group (Fig. 7A, right panels). After IRI in both vehicle- and PPTN-treated groups, while some PT cells showed a complete loss of AQP1 polarity with absent apical and basolateral staining after IRI (Fig. 7B; very damaged PTs), some cells showed partial redistribution with basolateral staining still visible (Fig. 7B; moderately damaged PTs). We quantified the number of intact, moderately damaged and very damaged PTs based on these AQP1 staining patterns, and found a significant reduction in the number of very damaged PTs together with an increase in the percentage of intact PTs and a decrease in the percentage of very damaged PTs in the treated groups compared to the untreated group 24h and 48h after IRI.

Deletion of the P2Y14 receptor in ICs confers kidney protection after IRI

To confirm the role of the P2Y14 receptor in ICs in renal inflammation and kidney damage leading to ischemic-induced AKI, we next generated an IC-specific P2Y14 receptor KO mouse by using the Cre-Lox system. Transgenic mice expressing Cre under the promoter of the V-ATPase B1 subunit (ATP6V1B1) in ICs ($B1^{Cre}$) (57, 58) were bred with P2Y14 receptor Lox mice (B6.129-P2ry14<tm1Gac>/Orl; EMMA, EM:05368). $B1^{Cre+}/P2Y14^{Flox/+}$ mice (IC KO) and $B1^{Cre-}/P2Y14^{Flox/+}$

(IC F/F; controls) were generated. Expression of *P2ry14* was assessed by quantitative PCR (qPCR) in ICs that were isolated by FACS based on their expression of the cell surface receptor c-Kit (CD117) (59). A negative selection for $CD45^+$ immune cells, which also express c-Kit, was performed (Fig. 8A; left panel, red dots). A significant reduction in *P2ry14* expression was observed in IC KO mice compared to IC F/F mice (Fig. 8A; right panel). IC KO and IC F/F mice were then subjected to bilateral IRI, as described above. Deletion of the P2Y14 receptor in ICs improved kidney function, illustrated by a reduction in the IRI-induced sCr elevation, compared to IC F/F mice (Fig. 8B), and reduced renal inflammation (Fig. 8C) 24h after IRI. Protection of renal tubule integrity was shown and quantified in H&E stained sections (Fig. 8E), and a protective effect of PTs was demonstrated in kidney sections labeled for AQP1 (Fig. 8F), or F-actin (Supp. Fig. 2). These results confirm the role of the P2Y14 receptor in ischemic-induced AKI.

Taken together, the results obtained in this pre-clinical AKI model show the participation of ICs in the rapid onset of renal inflammation, followed by renal dysfunction and PT damage following an ischemic insult. In our current model (Fig. 9), UDP-Glc levels are increased in the urine after renal IRI. Stressed PT epithelial cells, which are the most affected cell type in this model (and potentially other renal cell types), would release UDP-Glc, which then reaches the lumen of the collecting duct, where it activates the P2Y14 receptor located on the apical membrane of ICs. This stimulates the production of pro-inflammatory chemokines (PICs) by ICs, followed by rapid renal recruitment of neutrophils and monocytes. Consistent with our flow cytometry analysis, we found many neutrophils positive for N-elastase (Suppl. Fig. 3) or Ly6G (Suppl. Fig. 4) adjacent to PTs (positive for AQP1) in the DMSO group 24h post-IRI, and we showed that this neutrophil recruitment was strongly attenuated by PPTN. Very few neutrophils were detected in both sham groups (DMSO or PPTN). Many neutrophils were also detected near intact ICs 24h post-IRI in non-

treated mice, while very few neutrophils were detected in PPTN-treated mice (Suppl. Fig. 5). These inflammatory cells contribute to creating additional injury by invading PTs, and clogging the microvasculature of the kidney, which perpetuates and aggravates ischemic injury. We observed similar levels of moderate renal tubule damage at 2h post-IRI in both the DMSO and PPTN groups (Suppl. Fig. 6). Altogether, our results show that PPTN confers protection either by facilitating repair mechanisms in the renal tubules, and/or by attenuating further damage via reduction of post-ischemia renal inflammation. The latter possibility is supported by our data showing reduced numbers of apoptotic cells 24h post-IRI in the PPTN versus DMSO groups (Suppl. Fig. 7), as well as in the IC KO mice (Suppl. Fig. 8). Thus, blocking the P2Y14 receptor with a small molecule or deleting the receptor specifically in ICs significantly reduces the impact of IRI by reducing renal inflammation, preserving kidney function and reducing kidney tubule damage.

Urine UDP-glucose is elevated in ICU and cardiac surgery patients who develop AKI

Based on these pre-clinical model data, we next examined whether urinary levels of UDP-Glc in ICU patients could serve as a potential biomarker for AKI. A longitudinal pilot study was conducted using 108 urine samples collected from 35 patients. These urine samples were collected daily from patients admitted to the ICU for up to 8 days. Patient characteristics are displayed in Table 1. Briefly, median age was 73 years, 97% of enrolled patients were white and 26% were women. Twenty-six patients underwent elective cardiac-surgery requiring cardiopulmonary bypass, and five patients had sepsis. Figure 10A displays the peak urinary UDP-Glc concentration observed for each patient stratified by presence or absence of AKI (defined by at least 0.3mg/dL increase in sCr). In this cohort, 12 patients developed AKI (AKIN Stages 1, 2, 3) for an incidence of 34%. When patients progressed to a more advanced AKI during the hospital stay, the higher AKI

stage was used. Significantly higher urinary UDP-Glc concentrations were observed in patients who developed AKI versus patients who did not. At a cutoff value of 40nM, UDP-Glc predicted AKI with a sensitivity of 83.3% and specificity of 78.3% (positive predictive value of 66.7%; negative predictive value of 90.0%). When cardiac surgery patients were analyzed separately, similar statistic parameters were obtained (Fig. 10B), and at a cutoff value of 40nM, UDP-Glc predicted AKI with a sensitivity of 66.7% and specificity of 90.0% (positive predictive value of 66.7% and negative predictive value of 90.0%). Results of the Receiver Operator Characteristic (ROC) analysis are shown in Fig. 10C for all ICU patients (AUC 0.84; 95% CI 0.71, 0.97) and Fig. 10D for cardiac surgery patients only (AUC 0.91; 95% CI 0.77, 1.00). These results indicate that UDP-Glc is a promising actionable biomarker as a predictor of AKI due to its high sensitivity and specificity.

DISCUSSION

Here we report a major role for the UDP-Glc/P2Y14 receptor signaling pathway in driving early renal inflammation, leading to kidney dysfunction and proximal tubule damage following renal IRI. We show that inhibition of the P2Y14 receptor using a selective antagonist, or deletion of the IC P2Y14 receptor, confers strong kidney protection following bilateral renal IRI. The role of the P2Y14 receptor ligand UDP-Glc as a potential DAMP involved in acute kidney disease is supported by the strong correlation between UDP-Glc urinary levels and AKI diagnosis in ICU patients, with a particularly robust statistical association in cardiac surgery patients.

Using transgenic mice that express EGFP driven by the promoter of the IC specific V-ATPase subunit, ATP6V1B1, we characterized the transcriptomic profiles of medullary ICs under control conditions and following renal IRI. Under control conditions, we confirmed expression of several genes previously shown to be expressed in ICs by RNA sequencing of isolated ICs, as well as single-cell RNA sequencing (59). These include high expression levels of the transcription factor, *Foxi1,* the cell surface receptor *c-Kit*, the cytosolic enzyme carbonic anhydrase type 2 (*Car2)*, V-ATPase subunits including *Atp6v1e1, Atp6v1g3*, *Atp6v1b1, Atp6vod2* and *Atp6v1f* and *Atp6v1h*, the solute transporter *Slc26a4,* and the purinergic receptor *P2ry14.* Quantitative PCR and RNA-seq showed that following IRI, medullary ICs rapidly adopted a pro-inflammatory profile characterized by up-regulation of inflammatory mediators, including chemokines and cytokines. Whether cortical ICs also have a similar pro-inflammatory function will require additional studies. These results are in agreement with a previous study showing elevation of cytokines and chemokines in cells isolated by laser capture microdissection from different kidney regions (60). Interestingly, we found that

271 the *P2ry14* receptor itself was up-regulated after IRI, and we set out to investigate the role of the
272 UDP-Glc/P2Y14 receptor signaling pathway in the onset of AKI following renal IRI. We found that
273 UDP-Glc is rapidly excreted by the kidney following IRI, where it is positioned to activate apical
274 P2Y14 receptors. Importantly, PPTN is a small molecule that is excreted intact into the urine, and
275 so it is a suitable therapeutic compound for the prevention/alleviation of AKI. As described below,
276 PPTN has a protective effect not only in the kidney, but also in the lung and uterus, indicating its
277 multiple therapeutic potential.
278
279 We show here that renal infiltration of neutrophils and monocytes occurs rapidly, within
280 2h after IRI, in agreement with previous reports (27). Blocking this early response with PPTN
281 protects kidney function and reduces tubular damage, further supporting the notion that
282 inflammation is involved in the pathogenesis of AKI (14). The role of the P2Y14 receptor in
283 triggering renal inflammation following renal IRI is in agreement with our previous study showing
284 that a single intravenous injection of UDP-Glc is sufficient to cause renal neutrophil infiltration in
285 healthy mice (42). Other groups have also revealed the pro-inflammatory role of the P2Y14
286 receptor in different tissues including the lung and uterus (41, 43). Patients with cystic fibrosis
287 have elevated levels of UDP-Glc in their lung secretions, and instillation of UDP-Glc into the trachea
288 of WT mice induced lung neutrophil recruitment, a process that was inhibited by PPTN (43). The
289 P2Y14 receptor is expressed in the uterus epithelium, but not in the stroma, in human and mice,
290 and patients with pelvic inflammatory disease have elevated levels of P2Y14 receptor, IL-8 and IL-
291 1β in their endometrial epithelial lining (41). The renal IRI-induced increase in P2Y14 receptor
292 expression, together with elevated levels of CXCL1 and CXCL2 (the IL-8 murine homologs), IL-1β,
293 and other pro-inflammatory mediators, and the attenuated kidney damage in response to IRI that

we observed after silencing the P2Y14 receptor in ICs are in agreement with this previous study, which also showed that knocking down the P2Y14 receptor using siRNAs reduced the number of inflammatory neutrophils in the uterus (41). Collectively, these results indicate that UDP-Glc/P2Y14 receptor signaling occurs across species and that it acts at the luminal surface of organs that are in contact with the external environment. The high stability of UDP-Glc in the extracellular compartment, in contrast to other DAMPs, provides a mechanism by which high extracellular UDP-Glc levels could be achieved following stress and injury (35). This is supported by the rapid elevation of urinary UDP-Glc concentration that we detected after IRI.

The role of epithelial cells in mediating injury is rapidly emerging (17, 27). A previous study showed that alpha-ICs protect against urinary pathogenic bacteria by producing the bacteriostatic protein lipocalin 2 (also known as NGAL) (61). Our study provides additional evidence that ICs play a defense role in addition to their traditional role in the regulation of acid/base balance. A previous study showed that ischemic AKI activates the MAPK pathway (60). Interestingly, activation of P2Y14 receptor by UDP-Glc also activates this pathway further supporting its role in the initiation of AKI (35, 42). One of the transcripts that were up-regulated in ICs after IRI is IL-1β. This cytokine was recently implicated in the initiation and progression of tubulointerstitial fibrosis (62) and it is, therefore, possible that the increase in IL-1β that we show here might contribute to the progression of early inflammation towards fibrosis and might participate in the AKI to chronic kidney disease (CKD) transition. We also detected strong up-regulation of IL-34 in ICs, a cytokine that was recently implicated in the onset of AKI and worsening of subsequent CKD (63). While this article described the up-regulation of IL-34 by renal tubular cells 3 days after IRI,

316 the present study now shows that this cytokine transcript is rapidly up-regulated in ICs and could
317 participate in the very early response to AKI.
318
319 Other DAMPs produced in different clinical settings may also induce local organ
320 inflammation (64). For example, ATP, ADP and UDP are known DAMPS, and they may contribute
321 to the pathophysiology associated with ischemic AKI. Their contribution is tightly regulated by
322 extracellular ectonucleotidases, which metabolize ATP and ADP into adenosine (65). In addition,
323 some PPRs are located on the apical surface of tubular cells (e.g. Toll like receptors (TLRs), P2Y14
324 receptor, etc), and larger circulatory DAMPS such as the TLR ligand HGMB1 may not cross the
325 glomerular barrier to reach their target. The role of TLRs in AKI has been investigated by several
326 groups. TLR2 activation was proposed to promote PT repair following cisplatin-induced AKI (66,
327 67). Inhibition of TLR2 reduces myocardial ischemic-reperfusion injury in pigs (68). In the kidney,
328 while TLR2 and TLR4 expression is triggered by renal IRI, this increase is preceded by an
329 abrogation of TLR expression 1 and 6 hours after reperfusion (38, 69). This indicates that they are
330 probably not involved in the early phase of neutrophil and monocyte extravasation, which occurs
331 within 2h after IRI (this study and (27)). By contrast, P2Y14 receptor expression is high at baseline
332 and it further increases following IRI, and its ligand UDP-Glc is rapidly excreted by the kidney
333 indicating its readiness in initiating the very first steps in the inflammatory cascade that
334 accompanies AKI.
335
336 Bilateral renal IRI mimics the reduction in renal blood flow that occurs in different hospital
337 settings such as during a direct surgery to remove a kidney tumor, or during transportation of
338 transplanted kidneys. It also models the significant reduction in renal oxygenation that occurs

during a cardiac surgery requiring CPB. Indeed, it has been suggested that renal hypoxia secondary to a significant reduction in renal blood flow during CPB time plays a causative role in post-cardiac surgery AKI (CS-AKI) (12, 21). Moreover, heart ischemia occurs in addition to renal ischemia during a cardiac surgery requiring CPB, which would further contribute to the production of DAMPs. Thus, not only a local insult to the kidney, but damage to a remote organ such as the heart during surgery might play a role in CS-AKI. This is supported by the strong correlation that we observed between UDP-Glc and AKI in cardiac surgery patients, where both renal and heart ischemia may contribute to AKI via activation of the UDP-Glc/P2Y14 receptor signaling pathway.

Paradoxically, PTs do not express the P2Y14 receptor, but inhibition of this receptor in ICs protects them. The unique architecture of the kidney with collecting ducts, blood vessels and PTs all running in parallel with each other in the kidney medulla provides a unique morphological environment that is conducive to a cell-cell crosstalk between ICs and PTs. It is conceivable that chemokine production specifically in ICs, followed by massive immune cell infiltration, would affect neighboring PT cells, and thus inhibition of this process would reduce the impact of ischemia. Indeed, PTs have the ability to regenerate following ischemia (17), and they would do so more easily in the absence of harmful inflammatory cells. In support of this hypothesis, we observed similar increases in sCr, BUN and mALB/Cre 2h post-IRI in both the DMSO and PPTN groups. While sCr remained stable in the PPTN group, it continued to increase after 24h in the non-treated group. In addition, similar levels of moderate tubular damage were observed 2h post-IRI in the DMSO and PPTN groups, but the percentage of very damaged renal tubules (assessed in H&E sections) and PTs (assessed in AQP1-labeled sections) decreased in the PPTN group compared to DMSO 24h post-IRI. This was accompanied by a significant increase in the percentage of intact

tubules at 48h in the PPTN versus DMSO groups. In addition, the reduction in albuminuria and urinary KIM-1 levels that we observed at 48h post-IRI in the treated group compared to non-treated mice, indicated that PPTN attenuated the PT damage caused by IRI. Indeed, both an increased expression of KIM-1 and albuminuria have been previously attributed to PT injury (53, 54). Importantly 24h post-IRI, many neutrophils were found in close proximity to damaged PTs in the non-treated group, but very few were detected in the PPTN group. Altogether, these results indicate that PPTN confers renal tubule protection following IRI by either allowing repair mechanisms to occur, and/or by attenuating further damage via reduction of renal inflammation. The latter mechanism is supported by the reduced numbers of apoptotic cells that we detected 24h after IRI in the PPTN group versus DMSO.

AKI is a multifactorial disease, and targeted, patient-centered, approaches are now proposed to develop effective therapeutics. In this context, enrichment strategies based on biomarkers that are linked to the therapy being tested would allow intervention to a specific group of patients. This would yield a much larger effect size, a true benefit to therapeutics development programs. The fact that UDP-Glc is not only an indicator of AKI, but is also a causal marker that induces early renal inflammation, would provide the advantage of selecting patients that are likely to benefit from the use of a specific inhibitor that would block the UDP-Glc/P2Y14 receptor pro-inflammatory pathway. While the IC-specific baseline expression level of the P2Y14 receptor is high (this study and (59)), its increased expression following IRI makes it a likely player in the very early steps of inflammation. Importantly, ICs do not appear to be affected by IRI as they continue to show apical expression of the V-ATPase, in agreement with previous studies showing that collecting ducts are more resistant to ischemia compared to PTs (70). While the current work

supports the use of a P2Y14 receptor antagonist to prevent/attenuate AKI following a planned ischemic episode, additional studies will be required to determine whether this strategy could also be used in other clinical settings.

In conclusion, our study provides evidence that inhibiting the UDP-Glc/P2Y14 receptor pathway in ICs plays a protective role in kidneys submitted to an ischemic insult by targeting the early inflammation pathway, a prominent feature of AKI. Our observation that elevated urine levels of UDP-Glc are associated with AKI in ICU and cardiac surgery patients supports further investigation in humans to test the potential therapeutic benefits of inhibiting this pathway to prevent/alleviate AKI in hospital settings.

METHODS

This is a concise method section and additional information is provided in Suppl. Methods.

Animals

Adult C57BL/CBAF1 wild type male mice were purchased from Jackson Laboratories (Bar Harbor, ME, USA). Transgenic mice that express EGFP under the control of the promoter of the IC specific V-ATPase B1 subunit (ATP6V1B1) gene (71) were also used; they are referred to as B1-EGFP mice. Transgenic mice expressing Cre under the control the ATP6V1B1 promoter ($B1^{Cre}$) (57, 58) were bred with *p2ry14* Lox mice (B6.129-P2ry14<tm1Gac>/Orl; EMMA, EM:05368). $B1^{Cre+}$/ $p2ry14^{Flox/+}$ mice (IC KO) and $B1^{Cre-}$/ $p2ry14^{Flox/+}$ (IC F/F; controls) were generated.

Animal model of ischemia reperfusion injury (IRI)

Mice were housed in groups of three in metabolic cages (Tecniplast,West Chester, PA), and were acclimated to the metabolic cages for four days before the beginning of the experiment. They received 4-[4-(4-Piperidinyl)phenyl]-7-[4-(trifluoromethyl)phenyl]-2-naphthalenecarboxylic acid hydrochloride (PPTN-HCl; Tocris; Cat. No. 4862), or vehicle (DMSO). Mice were divided into four groups (SHAM-DMSO, SHAM-PPTN, IRI-DMSO and IRI-PPTN). For the 2h time point, mice were treated via a single injection through the tail vein, and for the 24h and 48h time points they were treated via osmotic minipumps (ALZET, Cupertino, CA), implanted subcutaneously, one day prior to the day of IRI surgery.

On the day of bilateral IRI surgery, mice were anesthetized with isofluorane the kidneys were exposed through flank incisions. The renal pedicle was clamped with an atraumatic vascular

clip during 35min. After the IRI surgery, animals were placed back into metabolic cages and allowed to recover for 2h, 4h, 24h or 48h post-surgery.

At the end of the experimental period, mice were anesthetized with Nembutal (60mg/kg body, i.p.), and a blood sample was collected from the left cardiac ventricle. Mice were perfused via the left cardiac ventricle with phosphate buffered saline (PBS) until kidneys were cleared of blood. The left kidney artery was clamped, and the left kidney was harvested and processed for flow cytometry analysis. The perfusion continued with paraformaldehyde-lysine-periodate fixative (PLP) as previously described (72). The right kidney was used for histopathology and immunofluorescence analysis.

UDP-glucose measurement by LC-MS/MS

UDP-glucose concentration was measured in mouse urine samples using the LC/MS/MS method performed at the Small Molecule Mass Spectrometry, Faculty of Arts and Sciences Harvard University (Cambridge, MA). The parameters used are listed in Suppl. Methods.

Isolation of EGFP$^+$ ICs from B1-EGFP mice, RNA extraction and RNA-seq.

Isolation of EGFP$^+$ ICs from the renal medulla of B1-EGFP mice was performed as we previously described (72). The RNA of EGFP$^+$ ICs from SHAM or IRI animals was isolated using PicoRNA KIT (Thermo Fisher Scientific). Each sample was obtained using 2 kidneys (from 2 mice). RNA-seq libraries were prepared using the Clontech SMARTER Kit v4, followed by sequencing on an Illumina HiSeq2500 instrument. Transcriptome mapping was performed with STAR (73) using the Ensembl annotation of mm9 reference genome. Read counts for individual genes were produced using HTSeq (74). Differential expression analysis was performed using the EdgeR

441 package (75) after normalizing read counts and including only those genes with CPM > 1 for one
442 or more samples. Differentially expressed genes were defined based on the criteria of >2-fold
443 change in expression value and P<0.05 and CV<1.2. Multiplot studio software was used to obtain
444 differential gene-expression. RNA seq dataset from SHAM and IRI ICs were deposited in the Gene
445 Expression Omnibus (GEO) website under accession number GS144522.
446
447 *Isolation of CD117^{+} CD45^{-} ICs*
448 Renal medulla single-cell suspensions were generated from B1^{Cre+}/*p2ry14*$^{Flox/+}$ mice (IC
449 KO) and B1^{Cre-}/*p2ry14*$^{Flox/+}$ mice (IC F/F; controls), as described in Suppl. Methods for the EGFP^{+}
450 IC isolation procedure. Cell suspensions were incubated with anti-mouse antibodies (1:100)
451 against PE/Cy7 CD117 (clone 2B8) and BV711 CD45 (clone 30-F11). FACS isolation of CD117^{+}
452 CD45^{-} ICs from the renal medulla was performed at the HSCI-CRM Flow Cytometry Core. The RNA
453 of CD177^{+} CD45^{-} ICs was isolated using PicoRNA KIT (Thermo Fisher Scientific). Each sample was
454 obtained using 2 kidneys (one mouse).
455
456 *Pro-inflammatory molecule expression in EGFP^{+} ICs by qPCR*
457 EGFP^{+} ICs were isolated by FACS from B1-EGFP mice 2h, 4h and 24h after IRI or sham
458 surgery, and total RNA was isolated from EGFP^{+} cells as described in Suppl. Methods. cDNA was
459 synthesized from 1000 pg RNA by using the SuperScript VILO cDNA Synthesis Kit (Invitrogen)
460 according to the manufacturer's instructions. Quantitative real-time PCR was performed by using
461 the Power SYBR Green PCR Master Mix (Life Technologies) and primers listed in Suppl. Table 4.
462 Results are reported as mean ± SEM using the formula -ΔCt= -[Ct target gene–Ct control gene

Gapdh]. Relative expression is derived from $2^{-\Delta\Delta Ct}$ where $-\Delta\Delta Ct = \Delta Ct$ treated group – mean of ΔCt control group.

PPTN measurement

The urine concentration of PPTN was quantified by LC/MS/MS at the Small Molecule Mass Spectrometry, Faculty of Arts and Sciences Harvard University, as described in detail in Suppl. Methods.

Flow cytometry analysis

Renal medulla single-cell suspensions were generated as previously described (72), and in Suppl. Methods. Cell suspensions were incubated with anti-mouse antibodies (1:100) against PE/Cy7 F4/80 (clone BM8), BV711 CD45 (clone 30-F11), APC/Cy7 CD11b (clone M1/711), FITC LY6C (clone AL-21), PE LY6G (clone 1A8), and Alexa Fluor® 647 CD64 (clone X54-5/7.1).

Measurement of urinary and serum markers of kidney function

Whole blood samples were allowed to clot 30 min at room temperature before centrifugation at 4,000g for 10min for collection of serum. Blood urea nitrogen (BUN) and serum creatinine (sCr) were measured using a Heska DriChem 7000 chemical analyser (Loveland, CO, https://www.heska.com/product/element-dc5x/), and urine creatinine and micro-albuminuria were measured using the DCA Vantage Analyzer (Siemens Healthineers, Norwood, MA), available at the Center for Comparative Medicine of MGH (Boston, MA). Urinary KIM-1 concentration was measured using the mouse KIM-1 ELISA (R&D Systems, Minneapolis, MN; cat. no.: MKM100).

Immunocytochemistry (H&E) and immunofluorescence

PLP-fixed kidney slices were processed for cryo-sectioning, immunocytochemistry and immunofluorescence. Kidney sections were labeled using hematoxylin and eosin (H&E), phalloidin (marker of F-actin), and antibodies against aquaporin 1 and megalin (PT markers), V-ATPase B1 subunit (IC marker), n-elastase and Ly6G (neutrophil markers) and cleaved caspase-3 (apoptotic marker), as described in detail in Suppl. Methods.

The percentage of intact, moderately damaged and very damaged renal tubules were quantified in H&E stained sections, and the percentage of intact, moderately damaged and very damaged PTs was quantified in AQP1-labeled sections by two investigators who were blinded to the study. The following AQP1 staining patterns were used: Intact PTs were identified when AQP1 was located in the brush-border and basolateral membrane. A complete loss of AQP1 polarity with absent apical and basolateral staining indicated very damaged PTs. A partial redistribution of AQP1 with basolateral staining still visible but loss of apical staining indicated moderately damaged PTs. The number of apoptotic cells was quantified by counting the number of cells positive for cleaved caspase-3 per area of tissue (16,900μm^2) in de-identified samples by two people.

ICU patient pilot study

This prospective pilot study was conducted at the Massachusetts General Hospital (MGH). Exclusion criteria were age under 18 years, pregnancy, long-term or acute dialysis, and organ transplantation within the prior year. Written informed consent was obtained from all study participants. Medical records were reviewed prospectively to retrieve baseline demographic

508 characteristics, pre-operative clinical and laboratory variables, including serial serum creatinine
509 measurements. Urine samples were freshly collected daily, and collection started the time of
510 arrival at the ICU for the patients not requiring cardiac surgery, or prior to surgery for the cardiac
511 surgery group.

512 Urine samples were centrifuged to remove cells and cell debris and urinary aliquots were
513 stored at -80 °C until assayed. Urinary UDP-Glc concentration was measured using the UDP-
514 glucose pyrophosphorylase-catalyzed conversion of UDP-glucose and ^{32}P-labeled pyrophosphate
515 (^{32}PPi) to [^{32}P]UTP and glucose-1P, as previously described (43, 76), and as detailed in Suppl.
516 Methods.

517

518 *Statistical analysis*

519 *Pre-clinical study:* The numeric data were analyzed using GraphPad Prism (Version 8; GraphPad
520 Software, La Jolla, CA, USA). Data were analyzed using Student's t test (two tailed), one-way
521 ANOVA, or two-way ANOVA followed by Tukey's or Dunnett's post hoc tests. A value of $P<0.05$ was
522 considered significant. Data were expressed as the means ± SEM. For each set of data, at least four
523 different animals were examined for each condition. Collection, analysis and interpretation of data
524 were conducted by at least two independent investigators, who were blinded to the study.

525

526 *Patient study:* Patient characteristics were described as median, interquartile range (IQR) for
527 continuous variables; counts and percentages for categorical variables. The differences between
528 patients who developed AKI and those who did not were compared using Wilcoxon rank-sum test,
529 Chi-squared test, and Fisher's Exact Test, as appropriate. We also drew the Receiver Operating
530 Characteristic (ROC) curves for all patients, and for cardiac surgery patients (77). A Chi-square

test was performed to compare the area under the ROC curve (AUC) to that of an intercept-only model, which has an AUC of 0.5. Analyses were conducted using SAS 9.4 and two-sided P values < 0.05 were considered as statistically significant.

Study approval

All pre-clinical procedures were approved by the Massachusetts General Hospital (MGH) Subcommittee on Research Animal Care and were performed in accordance with the *National Institutes of Health Guide for the Care and Use of Laboratory Animals* (Protocol #2015N000016). The patient pilot study was approved by the MGH institutional review board (Protocol #2015P000511).

AUTHOR CONTRIBUTIONS

MAB, ASA, SK, DB and SB designed the study; MAB, ACM, RGS, RNL, JS performed the experiments and analyzed the data; MAB, DB and SB wrote the manuscript; MAB, ACM, RGS, ASA, SK, SW, JVB, ERL, DB and SB read and commented on various drafts of the manuscript. RNL was trained in the laboratory of JVB in the renal IRI procedure.

ACKNOWLEDGMENTS

This work was supported by National Institutes of Health (NIH) grants HD040793 and 5U54HL119145 (to S.B.), R01DK121848 (to D.B.) and PO1 HL110873 (to ERL). S.B. is the recipient of the Richard Moerschner Endowed MGH Research Institute Chair in Men's Health. A.S.A is supported by American Heart Association award 18CDA34110131. The Microscopy Core facility of the Massachusetts General Hospital (MGH) Program in Membrane Biology receives support from Boston Area Diabetes and Endocrinology Research Center, grant DK57521 and Center for the Study of Inflammatory Bowel Disease, grant DK43351. The Zeiss LSM800 microscope was acquired using an NIH Shared Instrumentation Grant S10-OD-021577-01. We thank the HSCI-CRM Flow Cytometry Facility (MGH, Boston, MA), in particular Maris Handley and Amy Galvin Watt for their guidance and assistance in sorting and flow cytometry analysis.

CONFLICT OF INTEREST

Dr. Breton is a co-founder of Kantum Pharma (previously "Kantum Diagnostics, Inc."), a company developing a diagnostic and therapeutic combination to prevent and treat Acute Kidney Injury. Dr. Breton and her spouse own equity in the privately held company. Drs. Breton and Brown are inventors on a patent (United States Patent 10,088,489) covering technology that has

been licensed to the company through the MGH. Drs. Breton's and Brown's interests were reviewed and are managed by MGH and Partners HealthCare in accordance with their conflict of interest policies. The remaining others have no conflicts of interest to declare.

REFERENCES

1. Brown JR, Rezaee ME, Marshall EJ, and Matheny ME. Hospital Mortality in the United States following Acute Kidney Injury. *Biomed Res Int.* 2016:Article ID 4278579.
2. Kashani K, Rosner MH, Haase M, Lewington AJP, O'Donoghue DJ, Wilson FP, et al. Quality Improvement Goals for Acute Kidney Injury. *Clin J Am Soc Nephrol.* 2019;14(6):941-53.
3. Hoste EA, Bagshaw SM, Bellomo R, Cely CM, Colman R, Cruz DN, et al. Epidemiology of acute kidney injury in critically ill patients: the multinational AKI-EPI study. *Intensive Care Med.* 2015;41(8):1411-23.
4. Zuk A, and Bonventre JV. Recent advances in acute kidney injury and its consequences and impact on chronic kidney disease. *Current opinion in nephrology and hypertension.* 2019;28(4):397-405.
5. Lameire NH, Bagga A, Cruz D, De Maeseneer J, Endre Z, Kellum JA, et al. Acute kidney injury: an increasing global concern. *Lancet.* 2013;382(9887):170-9.
6. Siew ED, and Davenport A. The growth of acute kidney injury: a rising tide or just closer attention to detail? *Kidney international.* 2015;87(1):46-61.
7. Benoit SW, and Devarajan P. Acute kidney injury: emerging pharmacotherapies in current clinical trials. *Pediatr Nephrol.* 2018;33(5):779-87.
8. Hulse M, and Rosner MH. Drugs in Development for Acute Kidney Injury. *Drugs.* 2019;79(8):811-21.
9. Ostermann M, Liu K, and Kashani K. Fluid Management in Acute Kidney Injury. *Chest.* 2019;156(3):594-603.
10. Buglioni A, and Burnett JC, Jr. Pathophysiology and the cardiorenal connection in heart failure. Circulating hormones: biomarkers or mediators. *Clin Chim Acta.* 2015;443:3-8.
11. Harel Z, and Chan CT. Predicting and preventing acute kidney injury after cardiac surgery. *Current opinion in nephrology and hypertension.* 2008;17(6):624-8.
12. Lannemyr L, Bragadottir G, Krumbholz V, Redfors B, Sellgren J, and Ricksten SE. Effects of Cardiopulmonary Bypass on Renal Perfusion, Filtration, and Oxygenation in Patients Undergoing Cardiac Surgery. *Anesthesiology.* 2017;126(2):205-13.
13. O'Neal JB, Shaw AD, and Billings FTt. Acute kidney injury following cardiac surgery: current understanding and future directions. *Crit Care.* 2016;20(1):187.
14. Singbartl K, Formeck CL, and Kellum JA. Kidney-Immune System Crosstalk in AKI. *Semin Nephrol.* 2019;39(1):96-106.
15. O'Connor ME, Hewson RW, Kirwan CJ, Ackland GL, Pearse RM, and Prowle JR. Acute kidney injury and mortality 1 year after major non-cardiac surgery. *Br J Surg.* 2017;104(7):868-76.
16. Wang Y, and Bellomo R. Cardiac surgery-associated acute kidney injury: risk factors, pathophysiology and treatment. *Nat Rev Nephrol.* 2017;13(11):697-711.
17. Bonventre JV, and Yang L. Cellular pathophysiology of ischemic acute kidney injury. *J Clin Invest.* 2011;121(11):4210-21.
18. Ascione R, Lloyd CT, Underwood MJ, Gomes WJ, and Angelini GD. On-pump versus off-pump coronary revascularization: evaluation of renal function. *Ann Thorac Surg.* 1999;68(2):493-8.
19. Bucerius J, Gummert JF, Walther T, Schmitt DV, Doll N, Falk V, et al. On-pump versus off-pump coronary artery bypass grafting: impact on postoperative renal failure requiring renal replacement therapy. *Ann Thorac Surg.* 2004;77(4):1250-6.

20. Nigwekar SU, Kandula P, Hix JK, and Thakar CV. Off-pump coronary artery bypass surgery and acute kidney injury: a meta-analysis of randomized and observational studies. *Am J Kidney Dis.* 2009;54(3):413-23.
21. Ranucci M, Romitti F, Isgro G, Cotza M, Brozzi S, Boncilli A, et al. Oxygen delivery during cardiopulmonary bypass and acute renal failure after coronary operations. *Ann Thorac Surg.* 2005;80(6):2213-20.
22. Awad AS, Rouse M, Huang L, Vergis AL, Reutershan J, Cathro HP, et al. Compartmentalization of neutrophils in the kidney and lung following acute ischemic kidney injury. *Kidney international.* 2009;75(7):689-98.
23. Black LM, Lever JM, and Agarwal A. Renal Inflammation and Fibrosis: A Double-edged Sword. *J Histochem Cytochem.* 2019:22155419852932.
24. Lee SA, Noel S, Sadasivam M, Allaf ME, Pierorazio PM, Hamad ARA, et al. Characterization of kidney CD45intCD11bintF4/80+MHCII+CX3CR1+Ly6C- "intermediate mononuclear phagocytic cells". *PLoS One.* 2018;13(6):e0198608.
25. Lever JM, Hull TD, Boddu R, Pepin ME, Black LM, Adedoyin OO, et al. Resident macrophages reprogram toward a developmental state after acute kidney injury. *JCI Insight.* 2019;4(2).
26. Williams TM, Wise AF, Layton DS, and Ricardo SD. Phenotype and influx kinetics of leukocytes and inflammatory cytokine production in kidney ischemia/reperfusion injury. *Nephrology (Carlton).* 2018;23(1):75-85.
27. Basile DP, Anderson MD, and Sutton TA. Pathophysiology of acute kidney injury. *Compr Physiol.* 2012;2(2):1303-53.
28. Imig JD, and Ryan MJ. Immune and inflammatory role in renal disease. *Compr Physiol.* 2013;3(2):957-76.
29. Rabb H, Griffin MD, McKay DB, Swaminathan S, Pickkers P, Rosner MH, et al. Inflammation in AKI: Current Understanding, Key Questions, and Knowledge Gaps. *Journal of the American Society of Nephrology : JASN.* 2016;27(2):371-9.
30. Bolisetty S, and Agarwal A. Neutrophils in acute kidney injury: not neutral any more. *Kidney international.* 2009;75(7):674-6.
31. Bonventre JV, Basile D, Liu KD, McKay D, Molitoris BA, Nath KA, et al. AKI: a path forward. *Clin J Am Soc Nephrol.* 2013;8(9):1606-8.
32. Chen GY, and Nunez G. Sterile inflammation: sensing and reacting to damage. *Nature reviews Immunology.* 2010;10(12):826-37.
33. Kono H, and Rock KL. How dying cells alert the immune system to danger. *Nature reviews Immunology.* 2008;8(4):279-89.
34. Schaefer L. Complexity of danger: the diverse nature of damage-associated molecular patterns. *The Journal of biological chemistry.* 2014;289(51):35237-45.
35. Lazarowski ER, and Harden TK. UDP-Sugars as Extracellular Signaling Molecules: Cellular and Physiologic Consequences of P2Y14 Receptor Activation. *Molecular pharmacology.* 2015;88(1):151-60.
36. Lazarowski ER, Sesma JI, Seminario L, Esther CR, Jr., and Kreda SM. Nucleotide release by airway epithelia. *Sub-cellular biochemistry.* 2011;55:1-15.
37. Lazarowski ER, Shea DA, Boucher RC, and Harden TK. Release of cellular UDP-glucose as a potential extracellular signaling molecule. *Molecular pharmacology.* 2003;63(5):1190-7.
38. Wu H, Chen G, Wyburn KR, Yin J, Bertolino P, Eris JM, et al. TLR4 activation mediates kidney ischemia/reperfusion injury. *J Clin Invest.* 2007;117(10):2847-59.

39. Vallon V, Unwin R, Inscho EW, Leipziger J, and Kishore BK. Extracellular Nucleotides and P2 Receptors in Renal Function. *Physiol Rev.* 2020;100(1):211-69.
40. Sesma JI, Esther CR, Jr., Kreda SM, Jones L, O'Neal W, Nishihara S, et al. Endoplasmic reticulum/golgi nucleotide sugar transporters contribute to the cellular release of UDP-sugar signaling molecules. *The Journal of biological chemistry.* 2009;284(18):12572-83.
41. Arase T, Uchida H, Kajitani T, Ono M, Tamaki K, Oda H, et al. The UDP-glucose receptor P2RY14 triggers innate mucosal immunity in the female reproductive tract by inducing IL-8. *J Immunol.* 2009;182(11):7074-84.
42. Azroyan A, Cortez-Retamozo V, Bouley R, Liberman R, Ruan YC, Kiselev E, et al. Renal intercalated cells sense and mediate inflammation via the P2Y14 receptor. *PLoS One.* 2015;10(3):e0121419.
43. Sesma JI, Weitzer CD, Livraghi-Butrico A, Dang H, Donaldson S, Alexis NE, et al. UDP-glucose promotes neutrophil recruitment in the lung. *Purinergic signalling.* 2016;DOI 10.1007/s11302-016-9524-5.
44. Sesma JI, Kreda SM, Steinckwich-Besancon N, Dang H, Garcia-Mata R, Harden TK, et al. The UDP-sugar-sensing P2Y(14) receptor promotes Rho-mediated signaling and chemotaxis in human neutrophils. *Am J Physiol Cell Physiol.* 2012;303(5):C490-C8.
45. Zimmermann H. Extracellular metabolism of ATP and other nucleotides. *Naunyn-Schmiedeberg's archives of pharmacology.* 2000;362(4-5):299-309.
46. Chambers JK, Macdonald LE, Sarau HM, Ames RS, Freeman K, Foley JJ, et al. A G protein-coupled receptor for UDP-glucose. *The Journal of biological chemistry.* 2000;275(15):10767-71.
47. Breton S, and Brown D. Novel Proinflammatory Function of Renal Intercalated Cells. *Ann Nutr Metab.* 2018;72 Suppl 2:11-6.
48. Brown D, Lee R, and Bonventre JV. Redistribution of villin to proximal tubule basolateral membranes after ischemia and reperfusion. *Am J Physiol.* 1997;273(6 Pt 2):F1003-12.
49. Barrett MO, Sesma JI, Ball CB, Jayasekara PS, Jacobson KA, Lazarowski ER, et al. A selective high-affinity antagonist of the P2Y14 receptor inhibits UDP-glucose-stimulated chemotaxis of human neutrophils. *Molecular pharmacology.* 2013;84(1):41-9.
50. Jacobson KA, and Muller CE. Medicinal chemistry of adenosine, P2Y and P2X receptors. *Neuropharmacology.* 2016;104:31-49.
51. Sabbisetti VS, Waikar SS, Antoine DJ, Smiles A, Wang C, Ravisankar A, et al. Blood kidney injury molecule-1 is a biomarker of acute and chronic kidney injury and predicts progression to ESRD in type I diabetes. *Journal of the American Society of Nephrology : JASN.* 2014;25(10):2177-86.
52. Spiegel DM, Wilson PD, and Molitoris BA. Epithelial polarity following ischemia: a requirement for normal cell function. *Am J Physiol.* 1989;256(3 Pt 2):F430-6.
53. Han WK, Bailly V, Abichandani R, Thadhani R, and Bonventre JV. Kidney Injury Molecule-1 (KIM-1): a novel biomarker for human renal proximal tubule injury. *Kidney international.* 2002;62(1):237-44.
54. Wagner MC, Campos-Bilderback SB, Chowdhury M, Flores B, Lai X, Myslinski J, et al. Proximal Tubules Have the Capacity to Regulate Uptake of Albumin. *Journal of the American Society of Nephrology : JASN.* 2016;27(2):482-94.
55. Schwartz N, Hosford M, Sandoval RM, Wagner MC, Atkinson SJ, Bamburg J, et al. Ischemia activates actin depolymerizing factor: role in proximal tubule microvillar actin alterations. *Am J Physiol.* 1999;276(4):F544-51.

56. Sabolic I, Valenti G, Verbavatz JM, Van Hoek AN, Verkman AS, Ausiello DA, et al. Localization of the CHIP28 water channel in rat kidney. *Am J Physiol.* 1992;263(6 Pt 1):C1225-33.
57. Miller RL, Lucero OM, Riemondy KA, Baumgartner BK, Brown D, Breton S, et al. The V-ATPase B1-subunit promoter drives expression of Cre recombinase in intercalated cells of the kidney. *Kidney international.* 2009;75(4):435-9.
58. Nanami M, Pham TD, Kim YH, Yang B, Sutliff RL, Staub O, et al. The Role of Intercalated Cell Nedd4-2 in BP Regulation, Ion Transport, and Transporter Expression. *Journal of the American Society of Nephrology : JASN.* 2018;29(6):1706-19.
59. Chen L, Lee JW, Chou CL, Nair AV, Battistone MA, Paunescu TG, et al. Transcriptomes of major renal collecting duct cell types in mouse identified by single-cell RNA-seq. *Proc Natl Acad Sci U S A.* 2017;114(46):E9989-E98.
60. Xu K, Rosenstiel P, Paragas N, Hinze C, Gao X, Huai Shen T, et al. Unique Transcriptional Programs Identify Subtypes of AKI. *Journal of the American Society of Nephrology : JASN.* 2017;28(6):1729-40.
61. Paragas N, Kulkarni R, Werth M, Schmidt-Ott KM, Forster C, Deng R, et al. alpha-Intercalated cells defend the urinary system from bacterial infection. *J Clin Invest.* 2014;124(7):2963-76.
62. Lemos DR, McMurdo M, Karaca G, Wilflingseder J, Leaf IA, Gupta N, et al. Interleukin-1beta Activates a MYC-Dependent Metabolic Switch in Kidney Stromal Cells Necessary for Progressive Tubulointerstitial Fibrosis. *Journal of the American Society of Nephrology : JASN.* 2018;29(6):1690-705.
63. Baek JH, Zeng R, Weinmann-Menke J, Valerius MT, Wada Y, Ajay AK, et al. IL-34 mediates acute kidney injury and worsens subsequent chronic kidney disease. *The Journal of clinical investigation.* 2015;125(8):3198-214.
64. Meissner M, Viehmann SF, and Kurts C. DAMPening sterile inflammation of the kidney. *Kidney international.* 2019;95(3):489-91.
65. Eltzschig HK, Sitkovsky MV, and Robson SC. Purinergic signaling during inflammation. *N Engl J Med.* 2013;368(13):1260.
66. Sallustio F, Curci C, Aloisi A, Toma CC, Marulli E, Serino G, et al. Inhibin-A and Decorin Secreted by Human Adult Renal Stem/Progenitor Cells Through the TLR2 Engagement Induce Renal Tubular Cell Regeneration. *Sci Rep.* 2017;7(1):8225.
67. Andrade-Silva M, Cenedeze MA, Perandini LA, Felizardo RJF, Watanabe IKM, Agudelo JSH, et al. TLR2 and TLR4 play opposite role in autophagy associated with cisplatin-induced acute kidney injury. *Clin Sci (Lond).* 2018;132(16):1725-39.
68. Arslan F, Houtgraaf JH, Keogh B, Kazemi K, de Jong R, McCormack WJ, et al. Treatment with OPN-305, a humanized anti-Toll-Like receptor-2 antibody, reduces myocardial ischemia/reperfusion injury in pigs. *Circ Cardiovasc Interv.* 2012;5(2):279-87.
69. Wolfs TG, Buurman WA, van Schadewijk A, de Vries B, Daemen MA, Hiemstra PS, et al. In vivo expression of Toll-like receptor 2 and 4 by renal epithelial cells: IFN-gamma and TNF-alpha mediated up-regulation during inflammation. *J Immunol.* 2002;168(3):1286-93.
70. Witzgall R, Brown D, Schwarz C, and Bonventre JV. Localization of proliferating cell nuclear antigen, vimentin, c-Fos, and clusterin in the postischemic kidney. Evidence for a heterogenous genetic response among nephron segments, and a large pool of mitotically active and dedifferentiated cells. *J Clin Invest.* 1994;93(5):2175-88.
71. Miller RL, Zhang P, Smith M, Beaulieu V, Paunescu TG, Brown D, et al. V-ATPase B1 Subunit Promoter Drives Expression Of EGFP In Intercalated Cells Of Kidney, Clear Cells Of

Epididymis and Airway Cells of Lung In Transgenic Mice. *Am J Physiol Cell Physiol.* 2005;288(5):C1134-C44.
72. Battistone MA, Nair AV, Barton CR, Liberman R, Peralta MA, Capen D, et al. Extracellular adenosine stimulates Vacuolar ATPase-dependent proton secretion in medullary intercalated cells. *Journal of the American Society of Nephrology : JASN.* 2018;29:2.
73. Dobin A, Davis CA, Schlesinger F, Drenkow J, Zaleski C, Jha S, et al. STAR: ultrafast universal RNA-seq aligner. *Bioinformatics.* 2013;29(1):15-21.
74. Anders S, Pyl PT, and Huber W. HTSeq--a Python framework to work with high-throughput sequencing data. *Bioinformatics.* 2015;31(2):166-9.
75. Robinson MD, McCarthy DJ, and Smyth GK. edgeR: a Bioconductor package for differential expression analysis of digital gene expression data. *Bioinformatics.* 2010;26(1):139-40.
76. Lazarowski ER, Boucher RC, and Harden TK. Mechanisms of release of nucleotides and integration of their action as P2X- and P2Y-receptor activating molecules. *Molecular pharmacology.* 2003;64(4):785-95.
77. DeLong ER, DeLong DM, and Clarke-Pearson DL. Comparing the areas under two or more correlated receiver operating characteristic curves: a nonparametric approach. *Biometrics.* 1988;44(3):837-45.

FIGURE LEGENDS

Figure 1) Renal bi-lateral IRI increases urinary concentration of UDP-Glc. UDP-Glc was measured by LC-MS/MS in the urine of mice subjected to bi-lateral IRI and sham-operated mice. UDP-Glc concentration was normalized for urine creatinine (uCre). Each dot represents urine samples pooled from 3 mice. SHAM2h: n=7 samples (21 mice), SHAM24h: n=16 samples (48 mice), SHAM48h: n=6 samples (18 mice), IRI2h: n=13 samples (39 mice), IRI24h: n=7 samples (21 mice), IRI48h: n=6 samples (18 mice). Data are means ± SEM, analyzed using two-way ANOVA followed by a Tukey's post-hoc test. A significant elevation of UDP-Glc/uCre value was detected 2h after IRI compared to sham (IRI2h vs SHAM2h: *P=0.013). No difference was observed 24h and 48h after IRI. IRI2h vs IRI24h: P=0.0006, IRI2h vs IRI48h: P=0.0014.

Figure 2) Renal bi-lateral IRI increases expression of pro-inflammatory transcripts in ICs. **A)** Representative pseudoblot of EGFP^{+}ICs isolated by FACS from the kidney of B1-EGFP mice 2h after bi-lateral IRI. **B)** q-PCR showing expression of selected pro-inflammatory chemokines 2h, 4h and 24h after IRI or sham surgery (SHM). Each dot represents one mouse. No difference was detected in SHM-operated mice (2h, 4h and 24h) and all groups were then combined into a single SHM group. Data are means ± SEM, analyzed using one-way ANOVA followed by a Dunnett's post-hoc test. For *Cxcl1*: SHM (n=8), IRI2h (n=8), IRI4h (n=5), IRI24h (n=6); **P=0.0036, ****P<0.0001. For *Cxcl2*: SHM (n=6), IRI2h (n=10), IRI4h (n=6), IRI24h (n=6); *P=0.034, ***P=0.0009. For *Ccl2*: SHM (n=8), IRI2h (n=6), IRI4h (n=6), IRI24 h (n=6): *P=0.018, ***P=0.0006. For *Il1b*: SHM (n=7), IRI2h (n=8), IRI4h/IRI24h (n=6). For *Il6*: SHM (n=7), IRI2h (n=10), IRI4h/IRI24h (n=5). For *Ccl3*: SHM (n=7), IRI2h (n=9), IRI4h (n=5), IRI24h (n=6). For *Ccl4*: SHM (n=8), IRI2h (n=11),

IRI4h/IRI24h (n=6). For *Tnf and Ccl5*: SHM (n=8), IRI2h (n=10), IRI4h (n=5), IRI24h (n=6). **C)** Volcano plots (fold change (FC) versus P value) of gene expression profiles of ICs, isolated by FACS 2h after IRI (IRI IC) versus SHAM (CTR IC). Each sample of RNA (n=3) was obtained from a pool of 2 kidneys from 2 mice per group. The yellow line shows ± 2FC. Genes up-regulated after IRI are shown in red and genes down-regulated after IRI are shown in blue. The black dots represent transcripts that were not significantly differentially expressed. Data were analyzed using Student's t-test, two-tailed, and a value of $P<0.05$ was considered significant.

Figure 3) Inhibition of P2Y14 with PPTN attenuates IC-specific up-regulation of pro-inflammatory chemokines induced by IRI. A) Concentration of PPTN, a specific P2Y14 antagonist, in the urine of mice treated with a single i.v. injection corresponding to 0.18mg/kg (2h), or via continuous infusion with Alzet osmotic minipumps implanted s.c. for 24h or 48h corresponding to a dose of 4.55mg/kg/day, *versus* controls (CTR; treated with the vehicle only). PPTN urinary concentration was measured using LC-MS/MS. Data are means ± SEM analyzed using one-way ANOVA and a Dunnett's test. CTR vs 4.55mg/kg/day 24h ***P=0.0007, CTR vs 4.55mg/kg/day 48h ***P=0.0006. **B)** Quantitative PCR analysis of selected chemokines in ICs isolated by FACS 2h after IRI *versus* SHAM. PPTN-treated mice received a dose of 4.55 mg/kg/day through osmotic minipumps, non-treated mice received the vehicle. Data are means ± SEM, analyzed by one-way ANOVA and Tukey's test. No difference in chemokine expression was detected between the SHAM-vehicle and SHAM-PPTN groups, which were then combined into a single SHAM group (SHM). Some IRI groups are the same as those shown in Figure 2B (IRI2h). Each dot represents one mouse. For *Cxcl1*: SHM (n=6), IRI (n=8), IRI PPTN (n =8); ** P=0.0039, ***P=0.0002, ****P<0.0001. For *Cxcl2*: SHM (n=6), IRI (n=10), IRI PPTN (n=8); *P=0.013,

****P<0.0001. For *Ccl2*: SHM (n=8), IRI (n=8), IRI PPTN (n=8); **P=0.0092, ***P=0.0005. For *Il1b*: SHM (n=7) vs IRI (n=8) ***P=0.0006, IRI vs IRI PPTN (n=8) ***P=0.0006. For *Il6*: SHM (n=7), IRI (n=10), IRI PPTN (n=8); *P=0.042. For Cxcl10: SHM (n=4), IRI (n=6), IRI PPTN (n=7); *P=0.015. For *Il1f6*: SHM (n=3), IRI (n=5) and IRI PPTN (n=6). For *Tnf*: SHM (n=9), IRI (n=10) and IRI PPTN (n = 8) and for *Il34*: SHM (n=4), IRI (n=6) and IRI PPTN (n=7).

Figure 4) IRI induces the renal recruitment of pro-inflammatory immune cells, and this process is attenuated by PPTN. A) Flow cytometry analysis of renal recruitment of live $CD45^+$ immune cells (pink boxes) 2h post-IRI compared to SHAM. SHM DMSO (n=6), IRI DMSO (n=8), IRI PPTN(n=8); *P=0.037, **P=0.004, ****P<0.0001. **B)** Renal recruitment of live neutrophils ($CD45^+CD11b^+Ly6G^+$) relative to the live renal cell population (pink boxes) 2h post-IRI compared to SHAM. SHM DMSO (n=8), IRI DMSO (n=7), IRI PPTN (n=8); **P=0.0013, ***P = 0.0001, ****P<0.0001. **C)** Renal recruitment of live monocytes ($CD45^+CD11b^+Ly6C^+Ly6G^-$) relative to the live renal cell population (pink boxes) 2h post-IRI compared to SHAM (n=8 mice in each group). *P=0.048, ***P=0.0002. **D)** Renal recruitment of live neutrophils ($CD45^+CD11b^+Ly6G^+$) relative to the renal live cell population 24h (left panels; pink boxes) and 48h post-IRI compared to SHAM. SHM 24h DMSO (n=7), SHM 24h PPTN (n=7), SHM 48h DMSO (n=6), SHM 48h PPTN (n=6), IRI 24h DMSO (n=7), IRI 24h PPTN (n=6), IRI 48h DMSO (n=11), IRI 48h PPTN (n=10); *P=0.04, **P=0.0057, ****P<0.0001. **E)** Renal recruitment of live monocytes ($CD45^+CD11b^+Ly6C^+Ly6G^-$) relative to the live renal cell population 24h (left panels; pink boxes) and 48h post-IRI compared to SHAM. SHM 24h DMSO (n=7), SHM 24h PPTN (n=6), SHM 48h DMSO (n=6), SHM 48h PPTN (n=6), IRI 24h DMSO (n=6), IRI 24h PPTN (n=6), IRI 48h DMSO (n=11), IRI 48h PPTN (n=10). *P=0.039, ****P<0.0001. In all bar graphs, data are means ± SEM, and each dot represents one

mouse. Panels A, B, C: one-way ANOVA and Tukey's post-hoc test, Panels D, E: two-way ANOVA and Tukey's test.

Figure 5) PPTN protects kidney function post-IRI. A) Serum creatinine (sCre) over time post-IRI in vehicle-treated mice (DMSO) *versus* PPTN. Each dot represents one mouse. SHM DMSO (n=24), SHM PPTN (n=18), IRI2h DMSO (n=14), IRI2h PPTN (n=7), IRI24h DMSO (n=8), IRI24h PPTN (n=6), IRI48h DMSO (n=10), IRI48h PPTN (n=10). **P=0.0011, ****P<0.0001. **B)** BUN over time post-IRI. Each dot represents one mouse. SHM DMSO (n=24), SHM PPTN (n=18), IRI2h DMSO (n=14), IRI2h PPTN (n=7), IRI24h DMSO (n=8), IRI24h PPTN (n=6), IRI48h DMSO (n=10), IRI48h PPTN (n=8). *P=0.038, ****P<0.0001. **C)** Urine albumin-creatinine ratio (mALB/cre) over time post-IRI. Each dot represents urine collection from 3 mice. SHM DMSO (n=13, representing 39 mice), SHM PPTN (n=9; 27 mice), IRI2h DMSO (n=7; 21 mice), IRI2h PPTN (n=5; 15 mice), IRI24h DMSO (n=7; 21 mice), IRI24h PPTN (n=6; 18 mice), IRI48h DMSO (n=4; 12 mice), IRI48h PPTN (n=4; 12 mice). *P=0.047, ****P<0.0001. **D)** Urinary concentration of KIM-1 over time post-IRI. Each dot represents urine collection from 3 mice. SHM DMSO (n=6; 18 mice), SHM PPTN (n=6; 18 mice), IRI24h DMSO (n=6; 18 mice), IRI48h PPTN (n=3; 9 mice), IRI48h DMSO (n=4; 12 mice), IRI48h PPTN (n=3; 9 mice). *P=0.041, ****P<0.0001. For all graphs, data are means ± SEM, and two-way ANOVA followed by Tukey's test were performed.

Figure 6) PPTN protects kidney structure and renal tubules post-IRI. A) Kidney sections stained using hematoxylin and eosin (H&E) in SHAM, and 24h and 48h post-IRI. Right panels show higher magnification of the regions delineated by the boxes in the left panels. Severe alteration of renal tubule morphology is observed 24h and 48h post-IRI in the DMSO group. Protection of

kidney tubules is observed in the PPTN group *versus* DMSO at both time points post-IRI. No effect of PPTN alone was observed in the SHAM group. Scale Bar = 1mm, Inset Scale Bar =100μm. **B)** Quantification of the percentage of intact tubules (green bars), moderately damaged tubules with detectable cellular structures (blue bars), and very damaged tubules with a complete loss of cell architecture (red bars). SHAM DMSO (n=7 mice), SHAM PPTN (n=10), IRI24 h DMSO (n=7), IRI24h PPTN (n=6), IRI48h DMSO (n=7) and IRI48h PPTN (n=8). IRI24h DMSO vs IRI24h PPTN; *P=0.029, IRI48h DMSO vs IRI48h PPTN; *P=0.016 by two-way ANOVA followed by Tukey's post-hoc test. Between 940 and 1700 tubules were analyzed in each group.

Figure 7) PPTN maintains PT polarity post-IRI. A) Kidney sections labeled for AQP1 showed apical and basolateral localization in PTs from sham-operated mice. 24h and 48h post-IRI, a significant loss of AQP1 polarity was detected. In mice treated with PPTN, several PTs showed intact AQP1 localization at the brush-border and basolateral membrane. PPTN alone did not affect AQP1 distribution in sham-operated mice. Scale Bar = 1mm, Inset Scale Bar = 100μm. **B)** Quantification of the number of intact PTs with apical and basolateral AQP1 labeling (green bars), moderately damaged PTs with loss of apical labeling but detectable basolateral labeling (blue bars), and very damaged PTs with a complete loss of AQP1 polarity (red bars). PPTN induced a significant reduction in the number of very damaged PTs (IRI 24h DMSO (n=8) vs IRI 24h PPTN (n=6) **P=0.0043, and IRI 48h DMSO (n=11) vs IRI 48h PPTN (n=9) *P=0.011), together with an increase in the number of intact PTs 24h and 48h post-IRI (IRI 24h DMSO vs IRI 24h PPTN *P=0.026, and IRI 48h DMSO vs IRI 48h PPTN *P=0.012, compared to the untreated group. SHM DMSO (n=5) and SHM PPTN (n=4). Two-way ANOVA followed by a Tukey's post-hoc test was performed. Between 1500 and 3000 PTs were analyzed in each group.

Figure 8) Deletion of P2Y14 in ICs protects kidney function, reduces inflammation and attenuates damage post-IRI. A) Left: ICs ($CD117^{pos}CD45^{neg}$; red dots) were isolated from $B1^{Cre+}/P2Y14^{Flox/+}$ (IC KO) and $B1^{Cre-}/P2Y14^{Flox/+}$ (IC F/F; controls) mice. **Right:** *P2ry14* expression by q-PCR in IC KO *versus* IC F/F mice. ****P<0.0001 by unpaired two-tailed Student's t test (n=4). **B)** sCr 24h post-IRI versus sham in F/F and IC KO mice. *P=0.031, ***P=0.0008). **C)** Recruitment of $CD45^{+}CD11b^{+}Ly6G^{+}$24h post-IRI in F/F mice vs SHM (***P=0.0003), and attenuation in IC KO mice (IRI KO vs IRI F/F; *P=0.041). **D)** Recruitment of $CD45^{+}CD11b^{+}Ly6C^{+}Ly6G^{-}$ 24h post-IRI in F/F vs SHM (****P<0.0001), and attenuation in IC KO mice (IRI KO vs IRI F/F; *P=0.032). **P=0.0014. **E)** H&E staining of kidney of SHAM and 24h post-IRI in F/F and IC KO mice. Bar graph shows reduction of very damaged tubules (red bars; ***P=0.0002), and increase in intact tubules (green bars; **P=0.006) 24h post-IRI in KO versus F/F mice. Scale Bar = 50μm**. F)** AQP1 staining of kidney of SHAM and 24 h post-IRI in F/F and IC KO mice. Bar graph shows reduction of very damaged PTs (red bars: **P= 0.0012), and increase in intact PTs (green bars: **P=0.0093) 24h post IRI in IC KO versus F/F. Scale Bar = 50μm. Inset = 10μm. Data are means ± SEM. Each dot represents one mouse. Panels B,C,D: One-way ANOVA followed by Tukey's test. Panels E, F: Two-way ANOVA followed by Tukey's test. Panels B,C,D: n=5 for SHM F/F, SHM KO and IRI KO, and n=6 for IRI F/F. Panel E: n=6 for IRI F/F, SHM KO and IRI KO, and n=7 for SHM F/F. Panel F: n=6 mice for SHAM F/F, IRI24hF/F and IRI24hKO, and n=5 for SHAM KO. Between 1400 and 2500 tubules were analyzed per group (panels E and F).

Figure 9) Activation of P2Y14 in ICs triggers renal inflammation leading to PT injury. Renal ischemia induces the release of UDP-Glc from injured cells. UDP-Glc reaches the collecting duct lumen, where it binds P2Y14 located on the apical membrane of ICs. ICs then produce pro-

911 inflammatory chemokines (PICs), which attract circulating neutrophils and monocytes from the
912 blood vessel into the kidney stroma. Neutrophils and monocytes clog the microvasculature, and
913 extravasated cells attack proximal tubule cells, creating additional injury.
914
915 **Figure 10) Elevated UDP-Glc urinary levels are associated with AKI in ICU and cardiac**
916 **surgery patients. A)** Average peak urinary UDP-Glc concentration in ICU patients with AKI (ICU-
917 AKI, n=12) and without AKI (no-AKI, n=23). Significantly higher UDP-Glc concentration was
918 detected in patients who developed AKI *versus* patient who did not. **B)** Average peak urinary UDP-
919 Glc concentration in cardiac surgery patients with AKI (CS-AKI, n = 6) and without AKI (no-AKI, n
920 = 20). Significantly higher UDP-Glc concentration was detected in patients who developed AKI
921 *versus* patients who did not. **C)** Receiver operator characteristic (ROC) curve for the diagnosis of
922 AKI (Stage 1, 2 and 3 combined) in ICU patients. Peak UDP-Glc levels *versus* the higher AKI stage
923 for each patient were compared. **D)** Receiver operator characteristic (ROC) curve for the diagnosis
924 of AKI (Stage 1, 2 and 3 combined) in cardiac surgery patients. Data are expressed as median ±
925 interquartile range (IQR) for continuous variables from a cohort of 35 patients. Panels A and B)
926 Statistical analysis was performed using Wilcoxon rank-sum test, chi-squared test, and Fisher's
927 Exact Test. Panels C and D) A Chi-square test was performed to compare the area under the ROC
928 curve (AUC) to that of an intercept-only model, which has an AUC of 0.5. Two-sided P values < 0.05
929 were considered as statistically significant.
930

Table 1) Patient Characteristics

	All patients N = 35	**AKI** N = 12	**No AKI** N = 23	**P value**
Age (years)	73 [63, 82]	78 [71, 86]	68 [63, 82]	0.08
Female sex (%)	9 (26%)	1 (8%)	8 (35%)	0.22
White race (%)	34 (97%)	12 (100%)	22 (96%)	1.00
Reason for ICU admission (%)				0.04
Cardiac Surgery	26 (74%)	6 (50%)	20 (87%)	
Sepsis	5 (14%)	3 (25%)	2 (9%)	
Other	4 (11%)	3 (25%)	1 (4%)	
Baseline creatinine (mg/dL)	1 [0.9, 1.3]	1.2 [1.0, 1.6]	0.9 [0.8, 1.1]	0.04
Peak creatinine (mg/dL)	1.1 [0.9, 1.5]	1.8 [1.4, 2.8]	0.9 [0.8, 1.1]	<0.001

Continuous variables are presented as median [IQR].

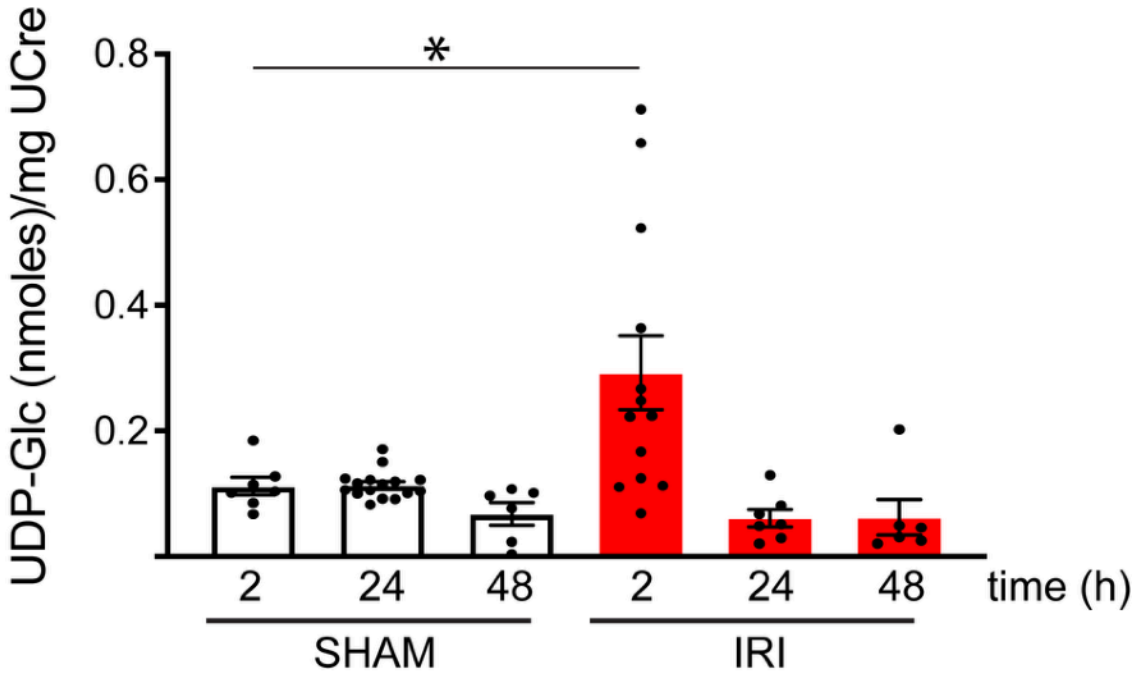

Figure 1) Renal bi-lateral IRI increases urinary concentration of UDP-Glc. UDP-Glc was measured by LC-MS/MS in the urine of mice subjected to bi-lateral IRI and sham-operated mice. UDP-Glc concentration was normalized for urine creatinine (uCre). Each dot represents urine samples pooled from 3 mice. SHAM2h: n=7 samples (21 mice), SHAM24h: n=16 samples (48 mice), SHAM48h: n=6 samples (18 mice), IRI2h: n=13 samples (39 mice), IRI24h: n=7 samples (21 mice), IRI48h: n=6 samples (18 mice). Data are means ± SEM, analyzed using two-way ANOVA followed by a Tukey's post-hoc test. A significant elevation of UDP-Glc/uCre value was detected 2h after IRI compared to sham (IRI2h vs SHAM2h: *P=0.013). No difference was observed 24h and 48h after IRI. IRI2h vs IRI24h: P=0.0006, IRI2h vs IRI48h: P=0.0014.

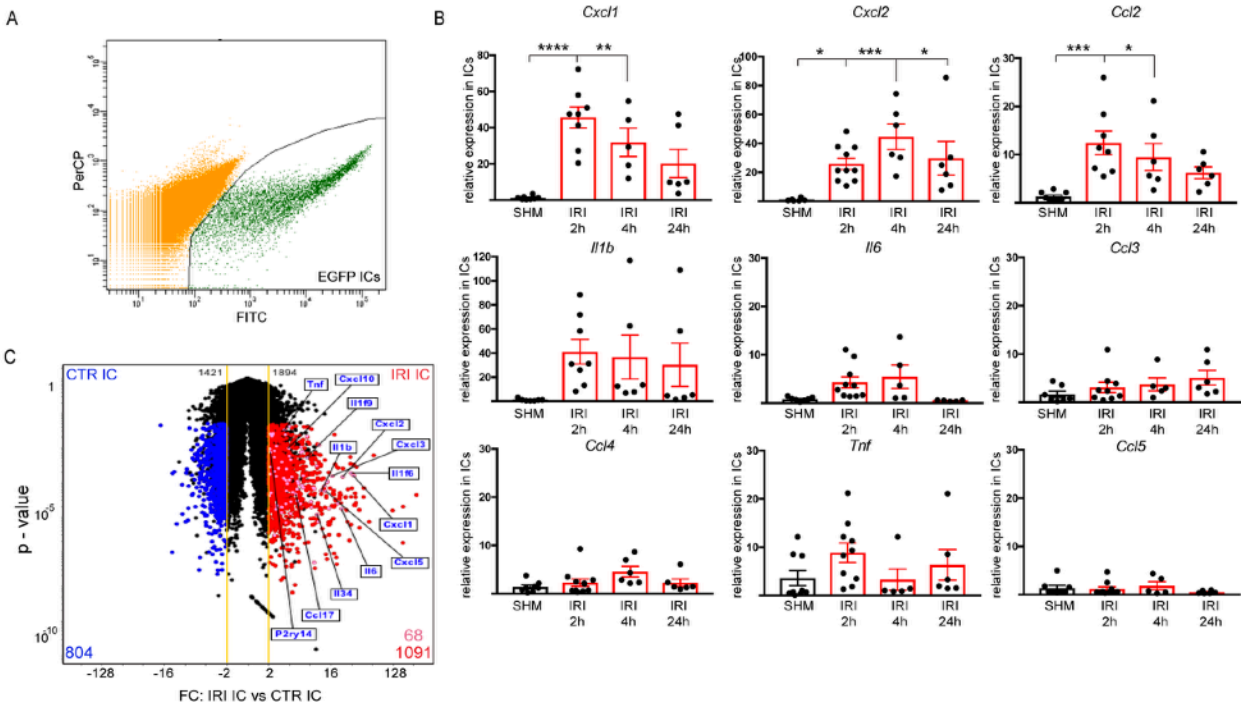

Figure 2) Renal bi-lateral IRI increases expression of pro-inflammatory transcripts in ICs. **A)** Representative pseudoblot of EGFP⁺ICs isolated by FACS from the kidney of B1-EGFP mice 2h after bi-lateral IRI. **B)** q-PCR showing expression of selected pro-inflammatory chemokines 2h, 4h and 24h after IRI or sham surgery (SHM). Each dot represents one mouse. No difference was detected in SHM-operated mice (2h, 4h and 24h) and all groups were then combined into a single SHM group. Data are means ± SEM, analyzed using one-way ANOVA followed by a Dunnett's post-hoc test. For *Cxcl1*: SHM (n=8), IRI2h (n=8), IRI4h (n=5), IRI24h (n=6); **P=0.0036, ****P<0.0001. For *Cxcl2*: SHM (n=6), IRI2h (n=10), IRI4h (n=6), IRI24h (n=6); *P=0.034, ***P=0.0009. For *Ccl2*: SHM (n=8), IRI2h (n=6), IRI4h (n=6), IRI24 h (n=6): *P=0.018, ***P=0.0006. For *Il1b*: SHM (n=7), IRI2h (n=8), IRI4h/IRI24h (n=6). For *Il6*: SHM (n=7), IRI2h (n=10), IRI4h/IRI24h (n=5). For *Ccl3*: SHM (n=7), IRI2h (n=9), IRI4h (n=5), IRI24h (n=6). For *Ccl4*: SHM (n=8), IRI2h (n=11), IRI4h/IRI24h (n=6). For *Tnf and Ccl5*: SHM (n=8), IRI2h (n=10), IRI4h (n=5), IRI24h (n=6). **C)** Volcano plots (fold change (FC) versus P value) of gene expression profiles of ICs, isolated by FACS 2h after IRI (IRI IC) versus SHAM (CTR IC). Each sample of RNA (n=3) was obtained from a pool of 2 kidneys from 2 mice per group. The yellow line shows ± 2FC. Genes up-regulated after IRI are shown in red and genes down-regulated after IRI are shown in blue. The black dots represent transcripts that were not significantly differentially expressed. Data were analyzed using Student's t-test, two-tailed, and a value of P<0.05 was considered significant.

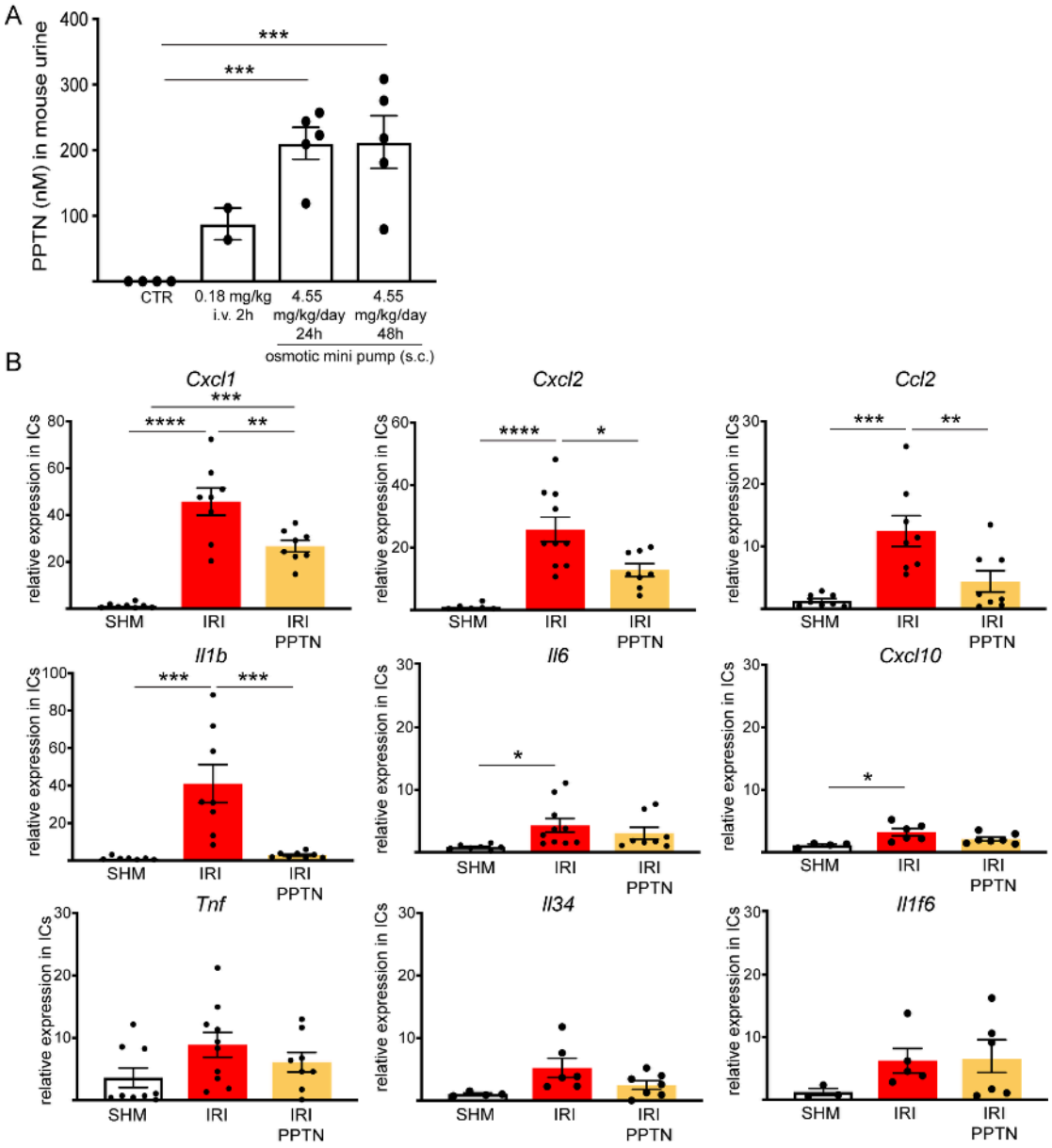

Figure 3) Inhibition of P2Y14 with PPTN attenuates IC-specific up-regulation of pro-inflammatory chemokines induced by IRI. A) Concentration of PPTN, a specific P2Y14 antagonist, in the urine of mice treated with a single i.v. injection corresponding to 0.18mg/kg (2h), or via continuous infusion with Alzet osmotic minipumps implanted s.c. for 24h or 48h corresponding to a dose of 4.55mg/kg/day, *versus* controls (CTR; treated with the vehicle only). PPTN urinary concentration was measured using LC-MS/MS. Data are means ± SEM analyzed using one-way ANOVA and a Dunnett's test. CTR vs 4.55mg/kg/day 24h ***P=0.0007, CTR vs 4.55mg/kg/day 48h ***P=0.0006. **B)** Quantitative PCR analysis of selected chemokines in ICs isolated by FACS 2h after IRI *versus* SHAM. PPTN-treated mice received a dose of 4.55 mg/kg/day through osmotic minipumps, non-treated mice received the vehicle. Data are means ± SEM, analyzed by one-way ANOVA and Tukey's test. No difference in chemokine expression was detected between the SHAM-vehicle and SHAM-PPTN groups, which were then combined into a single SHAM group (SHM). Some IRI groups are the same as those shown in Figure 2B (IRI2h). Each dot represents one mouse. For *Cxcl1*: SHM (n=6), IRI (n=8), IRI PPTN (n =8); ** P=0.0039, ***P=0.0002, ****P<0.0001. For *Cxcl2*: SHM (n=6), IRI (n=10), IRI PPTN (n=8); *P=0.013, ****P<0.0001. For *Ccl2*: SHM (n=8), IRI (n=8), IRI PPTN (n=8); **P=0.0092, ***P=0.0005. For *Il1b*: SHM (n=7) vs IRI (n=8) ***P=0.0006, IRI vs IRI PPTN (n=8) ***P=0.0006. For *Il6*: SHM (n=7), IRI (n=10), IRI PPTN (n=8): *P=0.042. For Cxcl10: SHM (n=4), IRI (n=6), IRI PPTN (n=7); *P=0.015. For *Il1f6*: SHM (n=3), IRI (n=5) and IRI PPTN (n=6). For *Tnf*: SHM (n=9), IRI (n=10) and IRI PPTN (n = 8) and for *Il34*: SHM (n=4), IRI (n=6) and IRI PPTN (n=7).

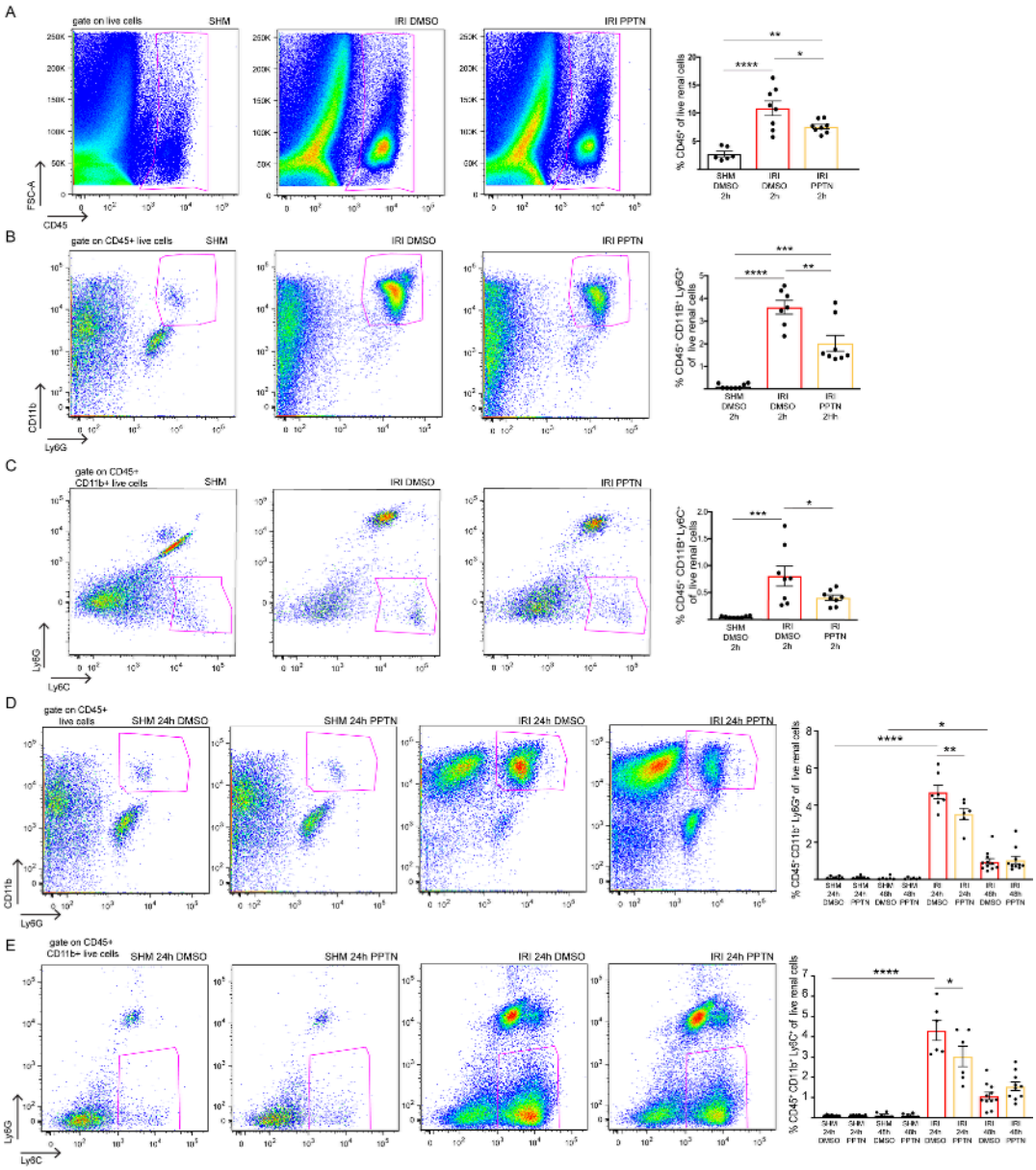

Figure 4) IRI induces the renal recruitment of pro-inflammatory immune cells, and this process is attenuated by PPTN. A) Flow cytometry analysis of renal recruitment of live CD45⁺ immune cells (pink boxes) 2h post-IRI compared to SHAM. SHM DMSO (n=6), IRI DMSO (n=8), IRI PPTN(n=8); *P=0.037, **P=0.004, ****P<0.0001. **B)** Renal recruitment of live neutrophils (CD45⁺CD11b⁺Ly6G⁺) relative to the live renal cell population (pink boxes) 2h post-IRI compared to SHAM. SHM DMSO (n=8), IRI DMSO (n=7), IRI PPTN (n=8); **P=0.0013, ***P = 0.0001, ****P<0.0001. **C)** Renal recruitment of live monocytes (CD45⁺CD11b⁺Ly6C⁺Ly6G⁻) relative to the live renal cell population (pink boxes) 2h post-IRI compared to SHAM (n=8 mice in each group). *P=0.048, ***P=0.0002. **D)** Renal recruitment of live neutrophils (CD45⁺CD11b⁺Ly6G⁺) relative to the renal live cell population 24h (left panels; pink boxes) and 48h post-IRI compared to SHAM. SHM 24h DMSO (n=7), SHM 24h PPTN (n=7), SHM 48h DMSO (n=6), SHM 48h PPTN (n=6), IRI 24h DMSO (n=7), IRI 24h PPTN (n=6), IRI 48h DMSO (n=11), IRI 48h PPTN (n=10); *P=0.04, **P=0.0057, ****P<0.0001. **E)** Renal recruitment of live monocytes (CD45⁺CD11b⁺Ly6C⁺Ly6G⁻) relative to the live renal cell population 24h (left panels; pink boxes) and 48h post-IRI compared to SHAM. SHM 24h DMSO (n=7), SHM 24h PPTN (n=6), SHM 48h DMSO (n=6), SHM 48h PPTN (n=6), IRI 24h DMSO (n=6), IRI 24h PPTN (n=6), IRI 48h DMSO (n=11), IRI 48h PPTN (n=10). *P=0.039, ****P<0.0001. In all bar graphs, data are means ± SEM, and each dot represents one mouse. Panels A, B, C: one-way ANOVA and Tukey's post-hoc test, Panels D,E: two-way ANOVA and Tukey's test.

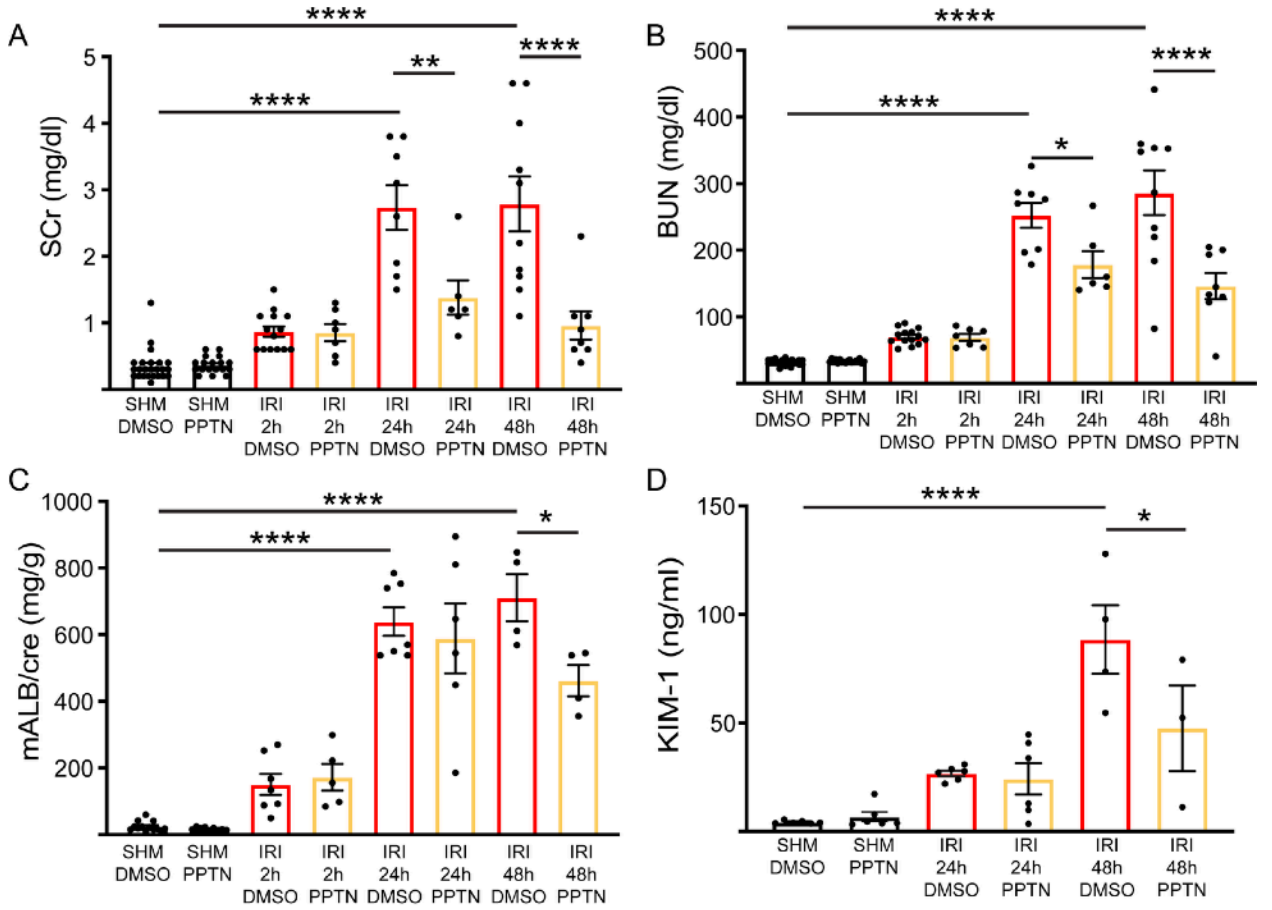

Figure 5) PPTN protects kidney function post-IRI. A) Serum creatinine (sCre) over time post-IRI in vehicle-treated mice (DMSO) *versus* PPTN. Each dot represents one mouse. SHM DMSO (n=24), SHM PPTN (n=18), IRI2h DMSO (n=14), IRI2h PPTN (n=7), IRI24h DMSO (n=8), IRI24h PPTN (n=6), IRI48h DMSO (n=10), IRI48h PPTN (n=10). **P=0.0011, ****P<0.0001. **B)** BUN over time post-IRI. Each dot represents one mouse. SHM DMSO (n=24), SHM PPTN (n=18), IRI2h DMSO (n=14), IRI2h PPTN (n=7), IRI24h DMSO (n=8), IRI24h PPTN (n=6), IRI48h DMSO (n=10), IRI48h PPTN (n=8). *P=0.038, ****P<0.0001. **C)** Urine albumin-creatinine ratio (mALB/cre) over time post-IRI. Each dot represents urine collection from 3 mice. SHM DMSO (n=13, representing 39 mice), SHM PPTN (n=9; 27 mice), IRI2h DMSO (n=7; 21 mice), IRI2h PPTN (n=5; 15 mice), IRI24h DMSO (n=7; 21 mice), IRI24h PPTN (n=6; 18 mice), IRI48h DMSO (n=4; 12 mice), IRI48h PPTN (n=4; 12 mice). *P=0.047, ****P<0.0001. **D)** Urinary concentration of KIM-1 over time post-IRI. Each dot represents urine collection from 3 mice. SHM DMSO (n=6; 18 mice), SHM PPTN (n=6; 18 mice), IRI24h DMSO (n=6; 18 mice), IRI48h PPTN (n=3; 9 mice), IRI48h DMSO (n=4; 12 mice), IRI48h PPTN (n=3; 9 mice). *P=0.041, ****P<0.0001. For all graphs, data are means ± SEM, and two-way ANOVA followed by Tukey's test were performed.

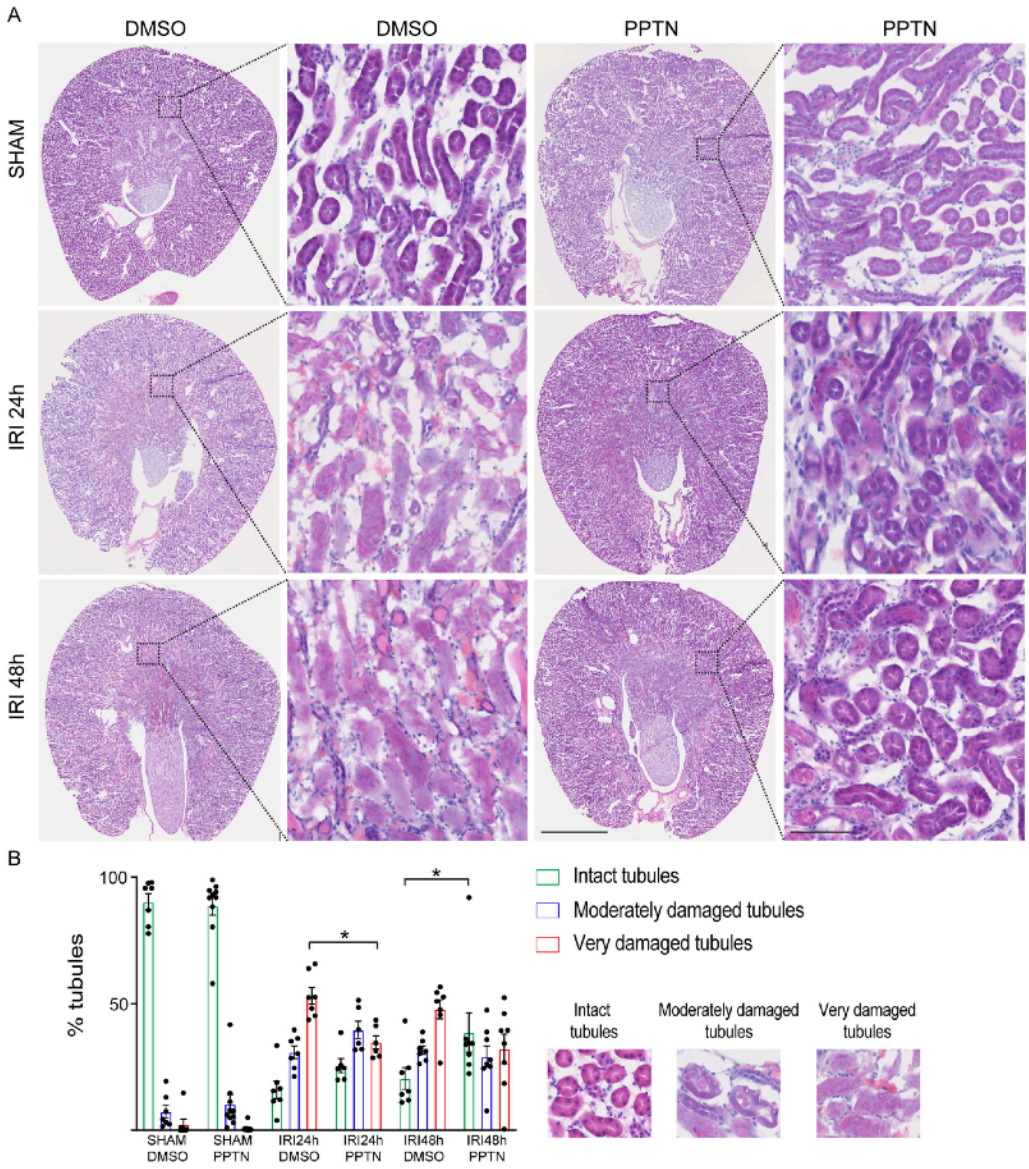

Figure 6) PPTN protects kidney structure and renal tubules post-IRI. A) Kidney sections stained using hematoxilin and eosin (H&E) in SHAM, and 24h and 48h post-IRI. Right panels show higher magnification of the regions delineated by the boxes in the left panels. Severe alteration of renal tubule morphology is observed 24h and 48h post-IRI in the DMSO group. Protection of kidney tubules is observed in the PPTN group *versus* DMSO at both time points post-IRI. No effect of PPTN alone was observed in the SHAM group. Scale Bar = 1mm, Inset Scale Bar =100µm. **B)** Quantification of the percentage of intact tubules (green bars), moderately damaged tubules with detectable cellular structures (blue bars), and very damaged tubules with a complete loss of cell architecture (red bars SHAM DMSO (n=7 mice), SHAM PPTN (n=10), IRI24 h DMSO (n=7), IRI24h PPTN (n=6), IRI48h DMSO (n=7) and IRI48h PPTN (n=8).). IRI24h DMSO vs IRI24h PPTN; *P=0.029, IRI48h DMSO vs IRI48h PPTN; *P=0.016 by two-way ANOVA followed by Tukey's post-hoc test. Between 940 and 1700 tubules were analyzed in each group.

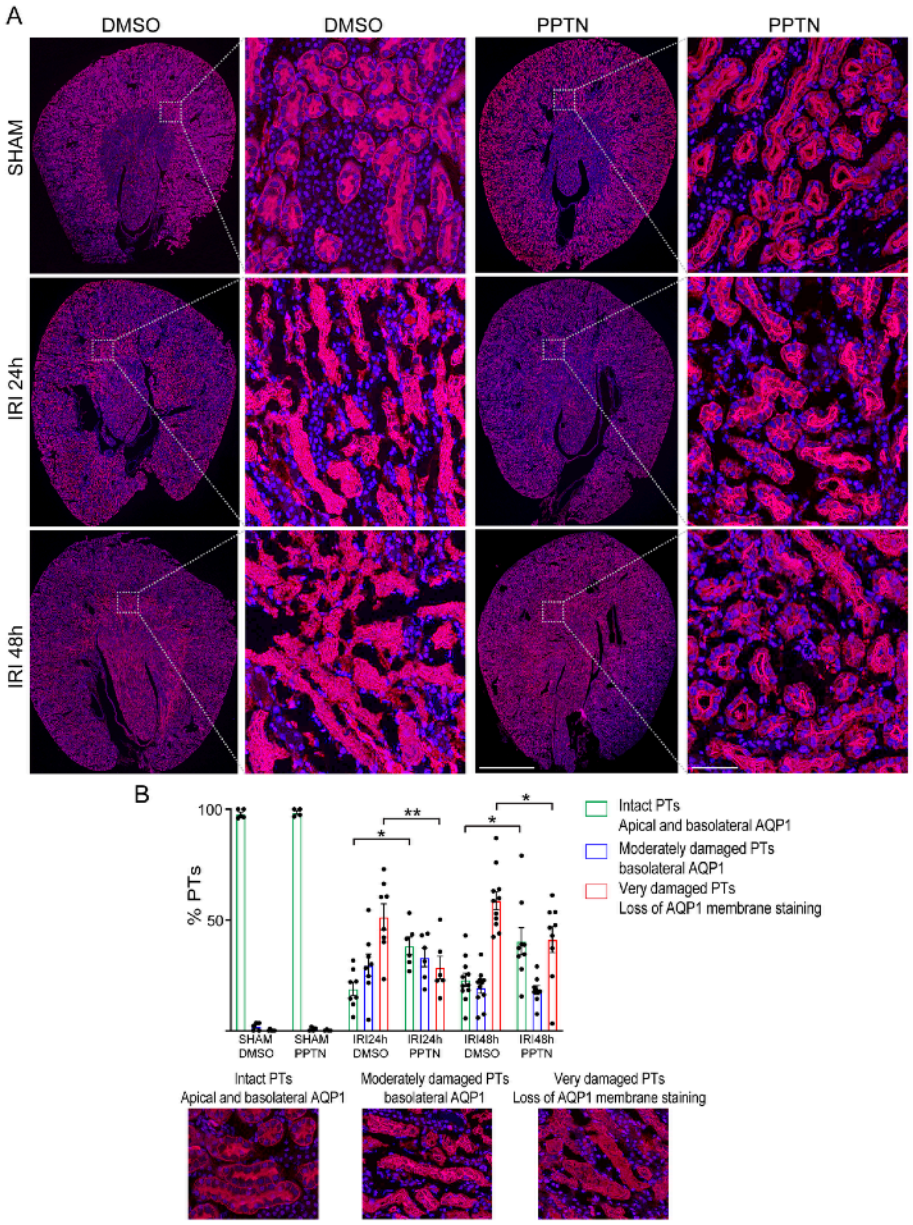

Figure 7) PPTN maintains PT polarity post-IRI. A) Kidney sections labeled for AQP1 showed apical and basolateral localization in PTs from sham-operated mice. 24h and 48h post-IRI, a significant loss of AQP1 polarity was detected. In mice treated with PPTN, several PTs showed intact AQP1 localization at the brush-border and basolateral membrane. PPTN alone did not affect AQP1 distribution in sham-operated mice. Scale Bar = 1mm, Inset Scale Bar = 100μm. **B)** Quantification of the number of intact PTs with apical and basolateral AQP1 labeling (green bars), moderately damaged PTs with loss of apical labeling but detectable basolateral labeling (blue bars), and very damaged PTs with a complete loss of AQP1 polarity (red bars). PPTN induced a significant reduction in the number of very damaged PTs (IRI 24h DMSO (n=8) vs IRI 24h PPTN (n=6) **P=0.0043, and IRI 48h DMSO (n=11) vs IRI 48h PPTN (n=9) *P=0.011), together with an increase in the number of intact PTs 24h and 48h post-IRI (IRI 24h DMSO vs IRI 24h PPTN *P=0.026, and IRI 48h DMSO vs IRI 48h PPTN *P=0.012), compared to the untreated group. SHM DMSO (n=5) and SHM PPTN (n=4). Two-way ANOVA followed by a Tukey's post-hoc test was performed. Between 1500 and 3000 PTs were analyzed in each group.

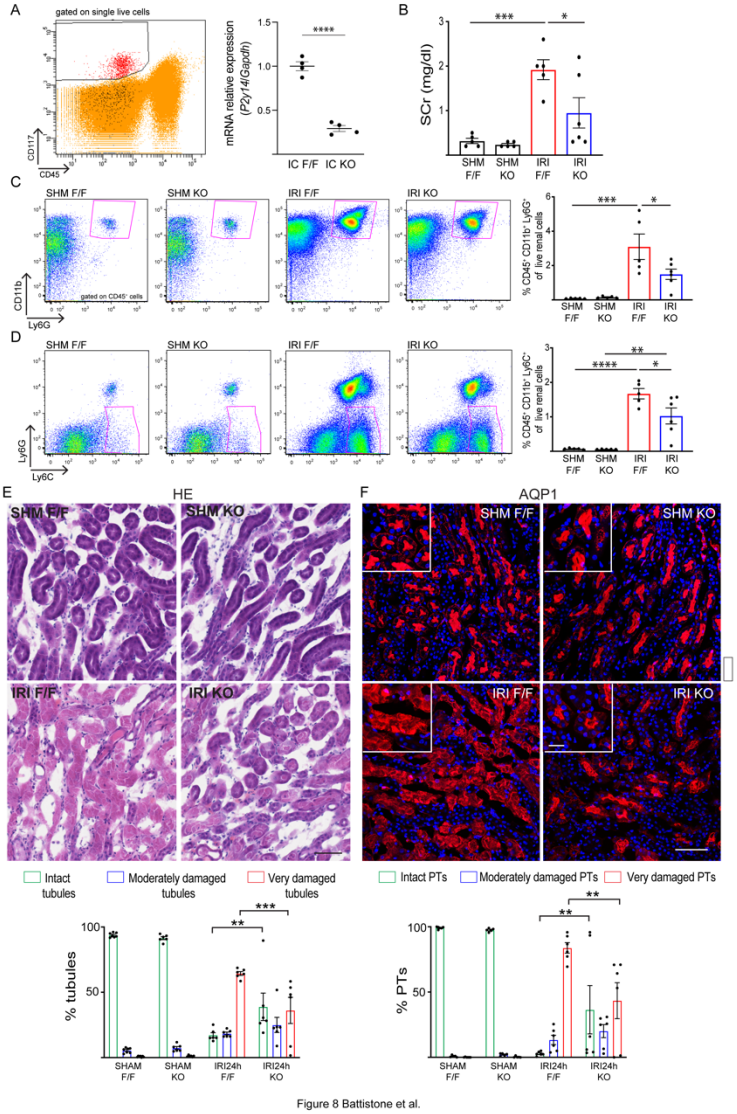

Figure 8 Battistone et al.

Figure 8) Deletion of P2Y14 in ICs protects kidney function, reduces inflammation and attenuates damage post-IRI. A) Left: ICs ($CD117^{pos}CD45^{neg}$; red dots) were isolated from $B1^{Cre+}/P2Y14^{Flox/+}$ (IC KO) and $B1^{Cre-}/P2Y14^{Flox/+}$ (IC F/F; controls) mice. **Right:** *P2ry14* expression by q-PCR in IC KO *versus* IC F/F mice. ****P<0.0001 by unpaired two-tailed Student's t test (n=4). **B)** sCr 24h post-IRI versus sham in F/F and IC KO mice. *P=0.031, ***P=0.0008). **C)** Recruitment of $CD45^{+}CD11b^{+}Ly6G^{+}$24h post-IRI in F/F mice vs SHM (***P=0.0003), and attenuation in IC KO mice (IRI KO vs IRI F/F; *P=0.041). **D)** Recruitment of $CD45^{+}CD11b^{+}Ly6C^{+}Ly6G^{-}$ 24h post-IRI in F/F vs SHM (****P<0.0001), and attenuation in IC KO mice (IRI KO vs IRI F/F; *P=0.032). **P=0.0014. **E)** H&E staining of kidney of SHAM and 24h post-IRI in F/F and IC KO mice. Bar graph shows reduction of very damaged tubules (red bars; ***P=0.0002), and increase in intact tubules (green bars; **P=0.006) 24h post-IRI in KO versus F/F mice. Scale Bar = 50µm**. F)** AQP1 staining of kidney of SHAM and 24 h post-IRI in F/F and IC KO mice. Bar graph shows reduction of very damaged PTs (red bars: **P= 0.0012), and increase in intact PTs (green bars: **P=0.0093) 24h post IRI in IC KO versus F/F. Scale Bar = 50µm. Inset = 10µm. Data are means ± SEM. Each dot represents one mouse. Panels B,C,D: One-way ANOVA followed by Tukey's test. Panels E, F: Two-way ANOVA followed by Tukey's test. Panels B,C,D: n=5 for SHM F/F, SHM KO and IRI KO, and n=6 for IRI F/F. Panel E: n=6 for IRI F/F, SHM KO and IRI KO, and n=7 for SHM F/F. Panel F: n=6 mice for SHAM F/F, IRI24hF/F and IRI24hKO, and n=5 for SHAM KO. Between 1400 and 2500 tubules were analyzed per group (panels E and F).

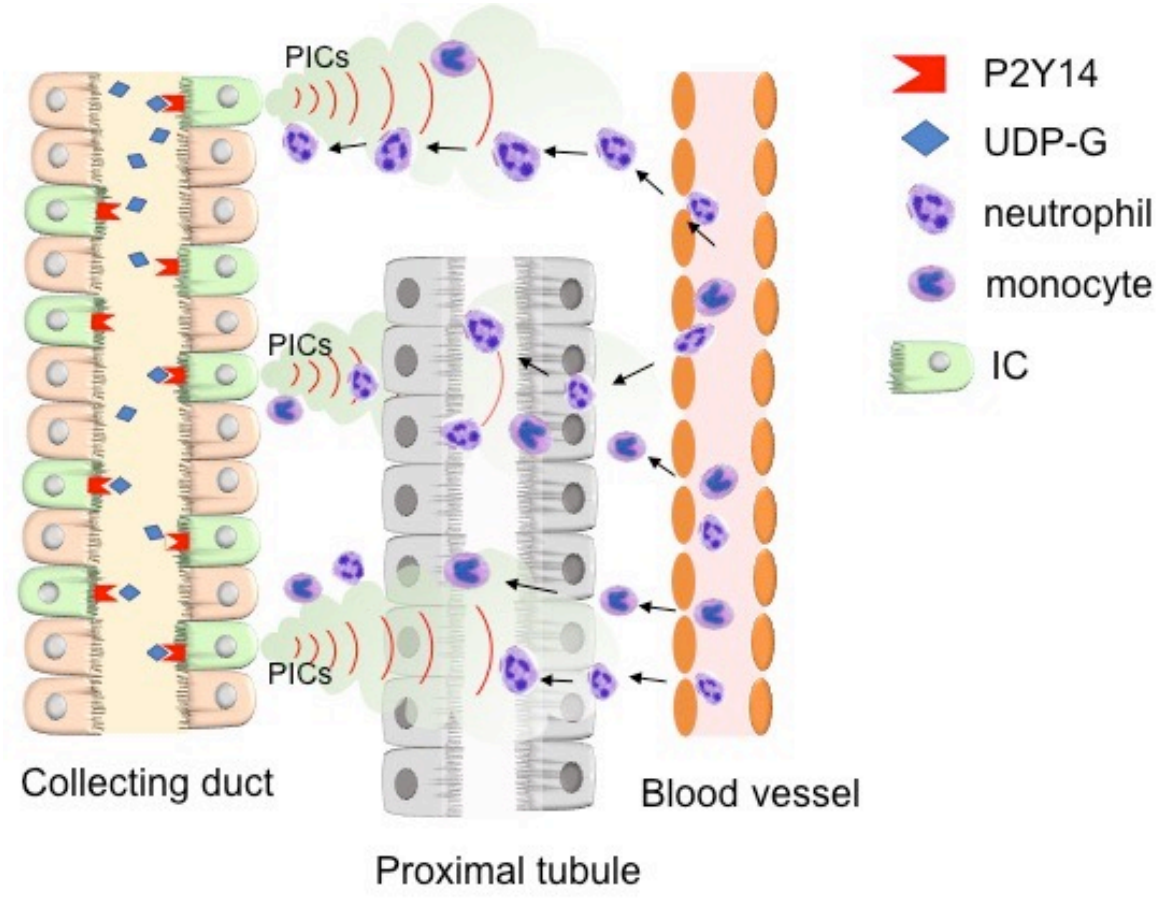

Figure 9) Activation of P2Y14 in ICs triggers renal inflammation leading to PT injury. Renal ischemia induces the release of UDP-Glc from injured cells. UDP-Glc reaches the collecting duct lumen, where it binds P2Y14 located on the apical membrane of ICs. ICs then produce pro-inflammatory chemokines (PICs), which attract circulating neutrophils and monocytes from the blood vessel into the kidney stroma. Neutrophils and monocytes clog the microvasculature, and extravasated cells attack proximal tubule cells, creating additional injury.

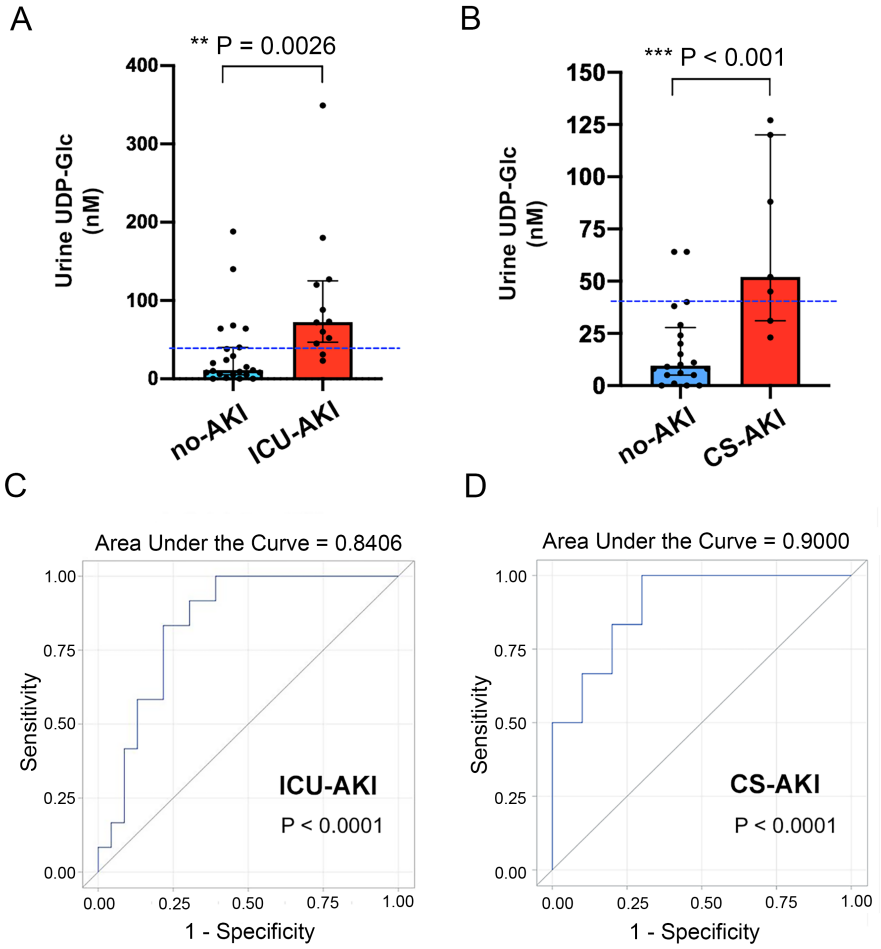

Figure 10) Elevated UDP-Glc urinary levels are associated with AKI in ICU and cardiac surgery patients. A) Average peak urinary UDP-Glc concentration in ICU patients with AKI (ICU-AKI, n=12) and without AKI (no-AKI, n=23). Significantly higher UDP-Glc concentration was detected in patients who developed AKI *versus* patient who did not. **B)** Average peak urinary UDP-Glc concentration in cardiac surgery patients with AKI (CS-AKI, n = 6) and without AKI (no-AKI, n = 20). Significantly higher UDP-Glc concentration was detected in patients who developed AKI *versus* patients who did not. **C)** Receiver operator characteristic (ROC) curve for the diagnosis of AKI (Stage 1, 2 and 3 combined) in ICU patients. Peak UDP-Glc levels *versus* the higher AKI stage for each patient were compared. **D)** Receiver operator characteristic (ROC) curve for the diagnosis of AKI (Stage 1, 2 and 3 combined) in cardiac surgery patients. Data are expressed as median ± interquartile range (IQR) for continuous variables from a cohort of 35 patients. Panels A and B) Statistical analysis was performed using Wilcoxon rank-sum test, chi-squared test, and Fisher's Exact Test. Panels C and D) A Chi-square test was performed to compare the area under the ROC curve (AUC) to that of an intercept-only model, which has an AUC of 0.5. Two-sided P values < 0.05 were considered as statistically significant.